POLITECNICO DI TORINO
Repository ISTITUZIONALE

Comparison of key performance indicators of sorbent materials for thermal energy storage with an economic focus

(Article begins on next page)

25 December 2024

Comparison of key performance indicators of sorbent materials for thermal energy storage with an economic focus

Letizia Aghemo[1], Luca Lavagna[1,*], Eliodoro Chiavazzo[2,*], Matteo Pavese[1]

[1]Department of Applied Science and Technology, Politecnico di Torino, Corso Duca degli Abruzzi 24, 10129, Torino, Italy

[2]Department of Energy, Politecnico di Torino, Corso Duca degli Abruzzi 24, 10129, Torino, Italy

*Corresponding authors E-mail(s): luca.lavagna@polito.it; eliodoro.chiavazzo@polito.it

Abstract

To expand the application scope of renewable energy sources, it is essential to further develop storage systems aimed at compensating the discrepancy in time between an energy-generation surplus and energy-demand peak. To this end, sorption thermal energy storage (STES) has recently gained interest for long-term (or seasonal) thermal energy storage. In the STES process, charging and discharging are typically based on reversible reactions between a solid sorbent and fluid (sorbate) that form the working pair. Sorbates are typically low-cost and environmentally safe fluids (e.g., water); however, the lack of robust and low-cost sorbent materials still creates a technological bottleneck for the long-term storage of thermal energy and, more generally, for sorption-based heat transformation. This study provides a general review of the existing sorbent–sorbate pairs, which consist of four main classes: liquids, solids, chemicals, and composite materials, with a special focus on their current costs. The results are presented in the form of several charts, which provide a comprehensive overview of sorbent materials in terms of their energy storage density (MJ/m^3), energy storage capacity (kJ/kg), and desorption temperature (i.e., charging temperature). In addition, novel charts are provided for a less explored parameter: the specific cost of current sorbents (expressed in kWh/€, which is the inverse of the storage capacity cost (SCC^{-1}). SCC^{-1} is a crucial figure of merit for a given sorbent because it affects the sorbent's real potential for widespread future applications.

Keywords: Sorption thermal energy storage; Sorbent; Sorbate

Contents

1. Thermal energy storage systems

The heating and cooling sector is responsible for half of all the consumed final energy in Europe, and most of the demand is met by the use of fossil fuels. More specifically, heating and cooling accounted for 68% of all European Union gas imports. As reported in [1], heating and cooling energy is exploited

for space heating (26%), water heating (5%), process heating (15%), and cooling (2%), and to a lesser extent, for cooking (2%) and space cooling (1%) (see **Figure 1)**. Approximately 45% of the energy utilized for heating and cooling in the European Union is used in the residential sector, 37% in industry, and 18% in services [2]. Thus, a significant reduction in the use of fossil fuels for heating and cooling purposes is a very effective way to achieve Europe's sustainability goals. However, the integration of renewable energy into cooling and heating systems requires new and affordable solutions, owing to their seasonal intermittent nature, as shown in **Figure 2**. Therefore, the massive exploitation of renewable energy sources requires the development of energy storage technologies that are capable of compensating for the discrepancy in time between the demand and energy peaks.
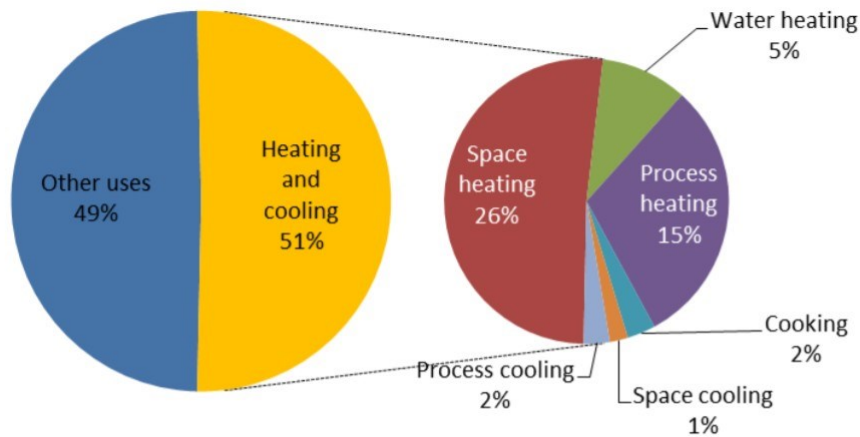
Figure 1: Pie chart representing the total heating and cooling demand of the European Union final energy consumption. Image sourced from [1]
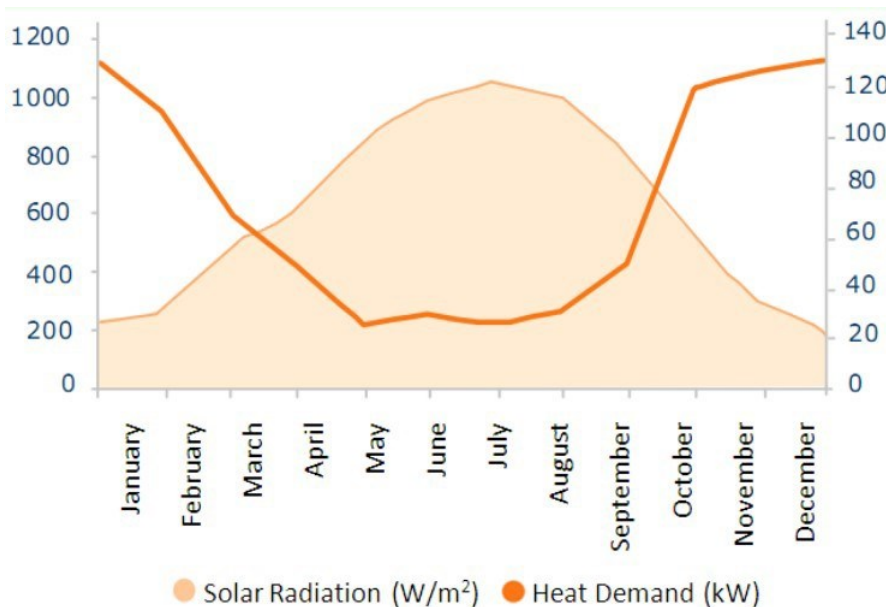
Figure 2: Graphic representation of solar radiation (W/m^2) and heat demand (kW), with solar radiation not matching the seasonal heat demand [3]

In thermal energy storage (TES) systems, the charging–discharging phases of a storage cycle are based on the ability of the materials to gain and release heat under desired conditions. These phases are used to distinguish between three types of TES technologies: sensible heat storage (SHS), latent heat storage (LHS), and thermochemical energy storage [4]. The latter is sometimes based on sorption phenomena and is therefore referred to as sorption thermal energy storage (STES) [5]. The working

principle of each system is shown in **Figure 3**, and a comparison of their expected performances is presented in **Figure 4**.

In SHS systems, thermal energy is stored by heating or cooling a liquid or solid storage medium, and water is the most common option [6]. Hence, thermal energy is stored as a function of the temperature difference between the storage medium and the environment, and the amount of stored energy depends on the heat capacity of the material. The main advantages are the cost-effectiveness of the system and the wide temperature range for various applications. However, SHS systems generally require a large volume of the storage medium, owing to its relatively low energy-storage capacity (although it depends on the adopted operating temperature, values in the order of 42000 kJ m^{-3} for water can be a reference). Moreover, these systems are usually unsuitable for medium-long (or seasonal) applications, owing to heat dissipation through the environment [7].

LHS systems utilize materials (commonly referred to as phase change materials – PCMs) that are capable of releasing or absorbing thermal energy while changing their phase. Their behavior strictly depends on the latent heat of the substance, that is, the heat required or released by a substance during a change in its physical state without a change in its temperature. PCMs include organic materials (paraffins, esters, alcohols), inorganic materials (salt hydrates, metals), and eutectic mixtures that combine two or more PCMs with similar melting and freezing points [8]. The phase change can involve either a solid-liquid, liquid-gas, or solid-solid transition, that is, from a crystal structure to a different structure. PCMs have typical energy storage capacities of 100–250 kJ kg^{-1} [9], and for low-temperature applications they are characterized by working temperatures of 0–100 °C [10]. PCMs benefit from the intrinsic isothermal character of heat discharge. However, more sophisticated approaches and designs (compared to that of the SHS system) are required to compensate for the low thermal conductivity of PCMs as well as for addressing supercooling or segregation that detrimentally affect the overall performance of the system [4,11,12].

In thermochemical energy storage and STES, the charging and discharging phases are based on reversible reactions between the sorbent material and corresponding sorbate. When combining the two elements of the working pair, heat is released, and their separation requires heat from the environment. STES systems have gained attention owing to their considerably high theoretical energy storage capacities, which can reach up to 4400 kJ kg^{-1} (referred to the material mass) [13]. Moreover, STES systems are unique in their ability to store heat for long periods of time without losing energy to the environment. Hence, this technology appears promising for the development of compact (seasonal) TES plants. Moreover, it has recently attracted increasing interest, as indicated by the number of publications in literature related to this topic shown in **Figure 5**. However, some important technical limitations still restrict this technology to the laboratory research stage, such as slow reaction kinetics, high working temperature (50–190 °C), and heat and mass-transfer high resistance within the sorbent material.
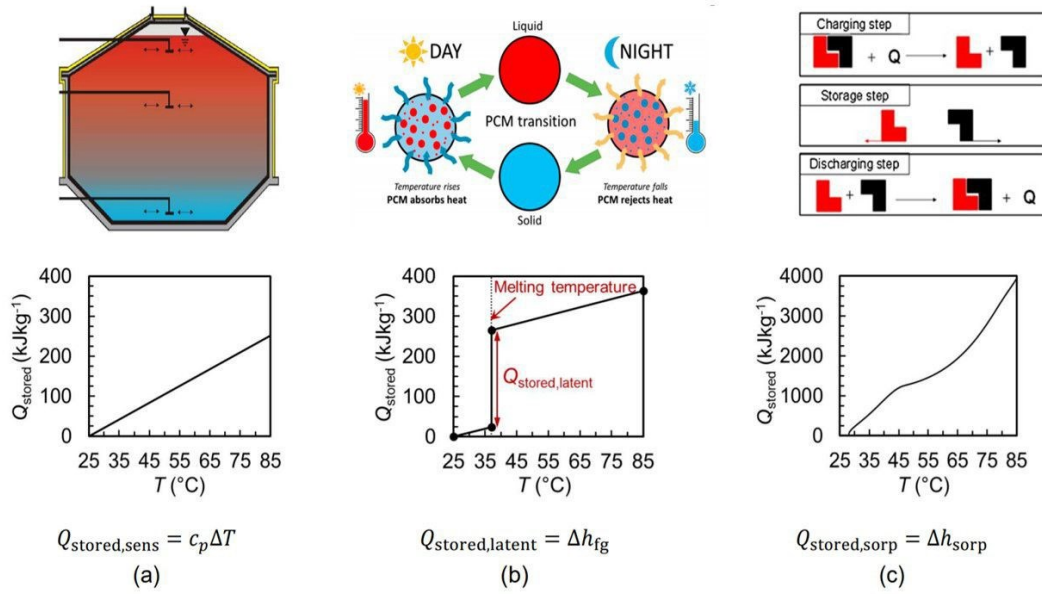
Figure 3: TOP: Schematic of different storage systems: (a) sensible heat storage, (b) latent heat storage, (c) sorption thermal energy storage. BOTTOM: (a) Stored specific heat versus temperature and the related thermodynamic equation for sensible TES (water at 25 °C), (b) latent heat ($C_{20}H_{42}$ with melting temperature of 37 °C), and (c) thermochemical energy storage (sorbent material Na_2S-H_2O, with heating rate of 1 K min^{-1} [14–17].

Figure 4: Energy storage capacities of PCMs (blue), sorption materials (green), and water (red line). PCM values are sourced from [18–20], and sorbent material values are from this study).

Figure 5: Number of scientific publications focused on sorption thermal energy storage (source: "Scopus")

The following sections detail the classification and characterization of the most suitable materials for STES and compare the performance of the most promising materials. It must be noted that the state of the art of STES systems is continuously being improved, but a standard guideline for the properties and choice of the most appropriate material is not present in the existing literature. Therefore, a clear comparison between previous studies is difficult. Hence, it is important to conduct a review of the general behavior and fundamental mechanisms of the sorption phenomena.
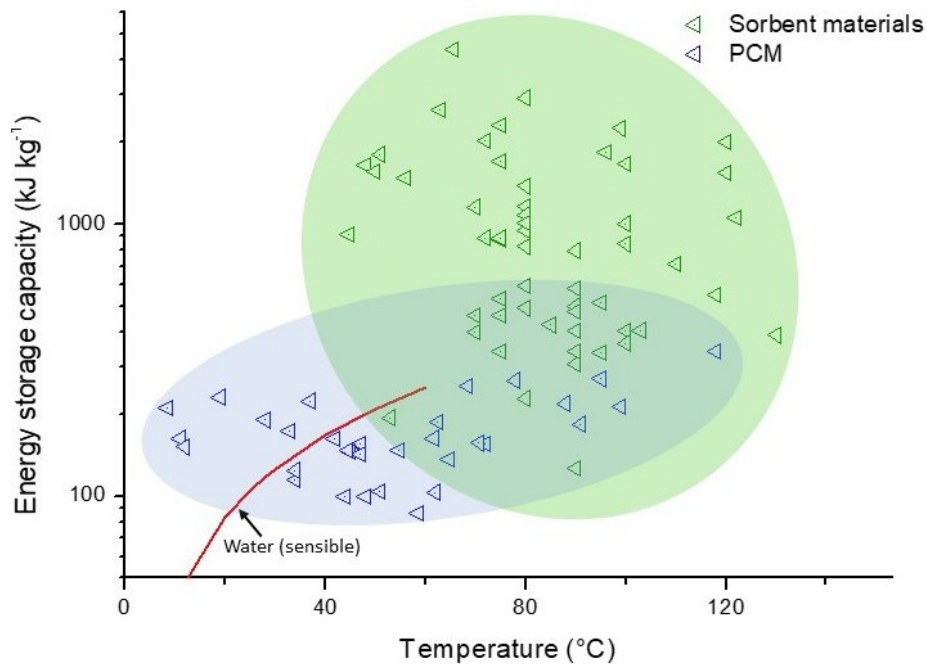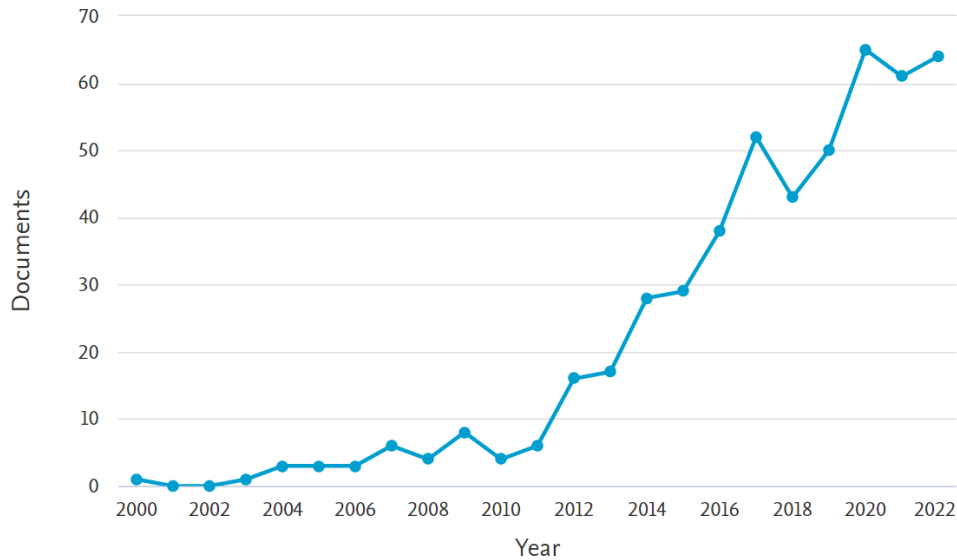
2. Sorption thermal energy storage

STES is based on a sorbent/sorbate working pair. When heat is provided to compound AB (sorbent+sorbate), it endothermically dissociates into two constituents, A and B, which can be stored without any energy loss, as long as the two elements are kept separate. Hence, this technology is promising for use in seasonal storage systems. However, when A and B are in contact, under proper operating conditions, the sorbate evaporates and reaches the sorbent; they exothermically form compound AB and concurrently release heat [21]. The overall mechanism is as follows:

$$A \cdot (m+n)B + \Delta H \rightarrow A \cdot mB + nB$$

It is worth noting that the term *sorption* refers to both *adsorption* and *absorption*. A schematic representation of these two mechanisms is shown in **Figure 6**. Adsorption is used when a solid surface (sorbent) tends to attract and retain molecules of other species (gas or liquid serving as a sorbate) with which the surface comes into contact. Absorption is a phenomenon in which the sorbate is not only retained on the surface, but it also passes through the surface and is distributed throughout the body of the solid or liquid [22]. Hence, adsorption is a surface phenomenon, whereas absorption is a bulk phenomenon. In adsorption, the concentration of adsorbed molecules is always greater in the immediate vicinity of the surface than in the free phase. In contrast, absorption involves the bulk penetration of molecules into the solid or liquid structure via diffusion.
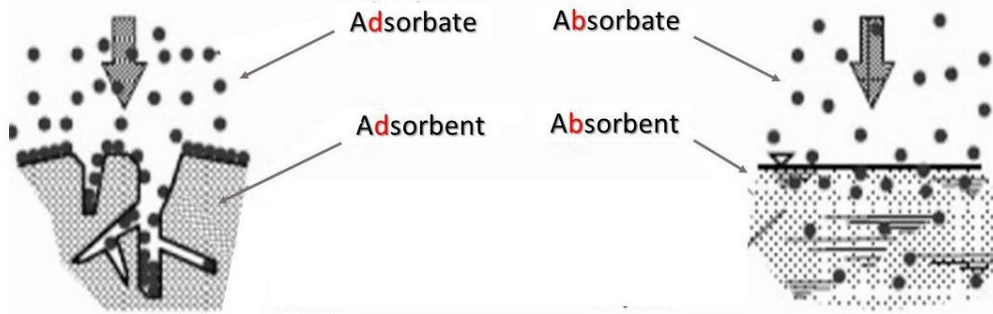
Figure 6: Schematic of the mechanism of adsorption (left) and absorption (right) [23]

2.1 Open or closed systems

A possible application of sorption heat-storage systems is a family house, which is characterized by space heating, domestic hot water demand, and solar thermal collectors on its roof that provide heat at the required desorption temperature [24]. STES systems can be divided into two categories: closed and open systems.

In closed systems (top panel of **Figure 7**), the sorbent and sorbate are isolated from the outdoor environment. During the charging process (sorbate desorption), a high thermal source heats the sorbent and enables the sorbate to be desorbed. Q_{ch} is the amount of heat required for complete desorption. The desorbed phase is condensed at temperature T_c and stored in a separate tank. The heat of condensation Q_c is rejected into the ambient environment. When the charging process ends, the condenser and reactor are disconnected. As long as the dry sorbent and sorbate are separated, heat preservation is a loss-free process. During the discharging process, the sorbate evaporates (by absorbing the heat of evaporation Q_{ev} from the outdoor environment) and flows into the sorbent material. Because sorption is an exothermic reaction, heat (Q_{dis}) is released into the reactor bed. The process can be defined as *closed* because the sorbate undergoes several evaporation-condensation cycles without mass exchange with the environment. **Figure 8** represents the ideal thermodynamic cycle of an adsorption heat storage process; the red lines represent the charging phase, whereas the blue lines represent the discharging phase. Ideally, sorbate adsorption/desorption occurs only during isobaric transformations.

In open systems (bottom panel of **Figure 7)**, water vapor (acting as the sorbate) is directly captured from the environment, and the released sorption heat is used to heat air, thereby avoiding the use of closed loops containing heat-transfer fluids. During the charging phase, hot and dry air flux enters the wet sorbent bed, which induces desorption. The air at the outlet is colder and has a higher humidity ratio than that at the inlet. In contrast, during discharging, humid and cold air flux enters the reactor with a dry sorbent. Water vapor from the air is adsorbed, which induces heat release. Therefore, the air temperature increases and its humidity ratio decreases. In this case, the performance of the storage system is strictly related to the inlet relative humidity (RH) of the air. Helaly *et al.* [25] observed the effect of RH on system performance and noted an increase in the energy storage density (ESD) with increasing RH%. Both types of systems have advantages and disadvantages. Open systems are relatively simple, less expensive, and easy to maintain. However, they are characterized by important technical disadvantages. The system performance is significantly affected by the thermo-hygrometric conditions of the outdoor air, which impose critical geographical constraints on the use of this technology. Moreover, no hazardous materials can be adopted as sorbates, owing to the mass exchange with the environment. Finally, if the air at the outlet of the system is sent directly to a room, thermo-hygrometric conditions can be perturbed, which affects the thermal comfort of people in the room. In contrast, closed systems are not subject to geographical and material constraints, thereby

offering a considerably higher degree of flexibility. In addition, the condensation heat can be recovered. However, the system presents more structural complexity because heat exchangers are required to provide or extract heat from/to the sorbent and the evaporator/condenser. Consequently, both the cost and volume of the system increase [5 Water vapor
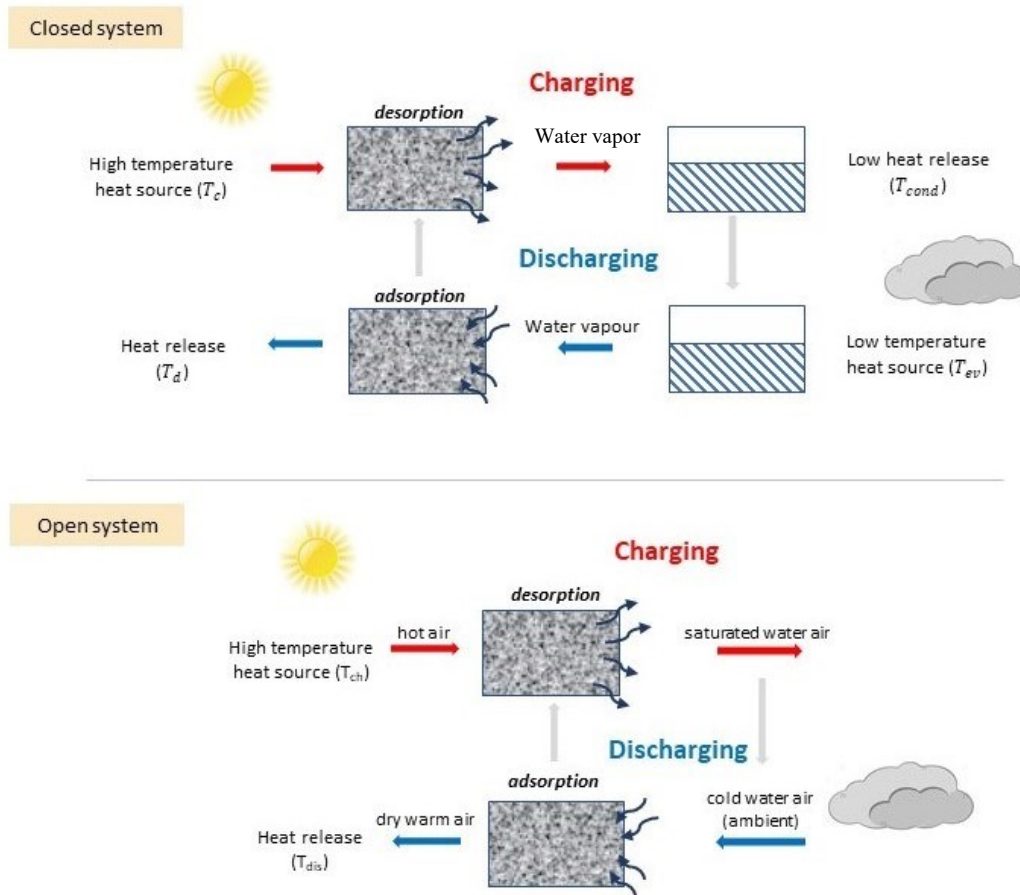
Figure 7: Above, schematic of a generic closed system. In red, the charging cycle: the heat source (sun) heats the sorbent, which leads the sorbate (water) to evaporate and subsequently condense. In blue, the discharging cycle: the sorbent evaporates and flows into the sorbent material, with heat release. Below, schematic of a generic open system. In red, the charging cycle: dry hot air flux enters the wet sorbent, which induces water desorption. In blue, the discharging cycle: humid air flows into the sorbent material, with heat release.
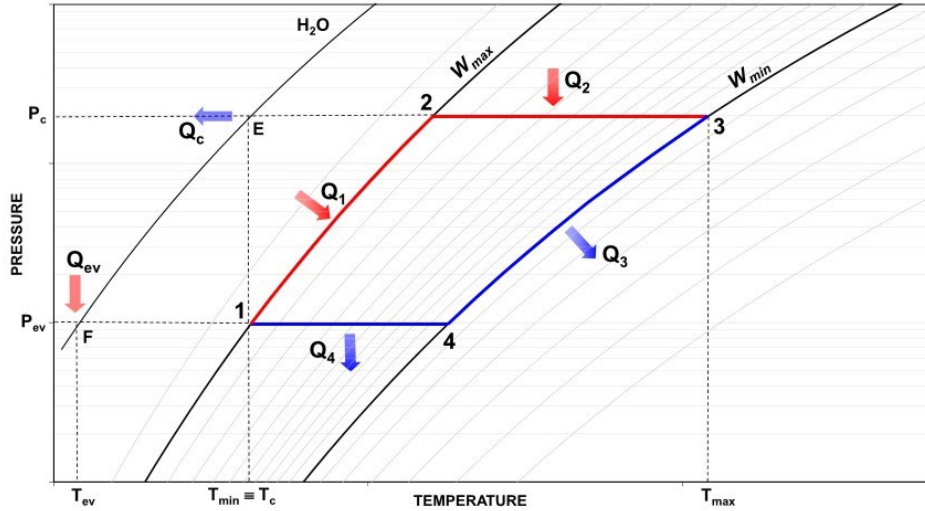
Figure 8: Ideal thermodynamic working cycle of a closed adsorption heat storage process: the red lines represent the charging phase (i.e. isosteric heating and isobaric desorption), whereas the blue lines indicate the discharging phase (i.e. isosteric cooling and isobaric adsorption). In a typical seasonal application, T_{ev}, T_c, and T_{max} represent the winter mean temperature, summer mean temperature, and maximum temperature of the heat source, respectively [26]

2.2 Selection criteria and relevant key performance indicators

Sorption materials form the basis for designing STES systems, and their properties strictly define the potential of the system. Key performance indicators (KPI) are widely recognized as crucial factors when comparing different solutions in a specific field. *Palomba et al.* [27] investigated the definition of KPIs for TES systems in depth. They highlighted the variety of KPI proposals in the literature and concluded that the definition of a unique set of suitable describing parameters is difficult. However, after evaluating and comparing different systems, they presented only a few KPIs as the most relevant ones, which the authors of this study are in agreement with. The selected KPIs, which help to better understand the potential of different solutions, are as follows.

Energy storage density. Among the most important KPIs of sorbent materials for TES applications, it is worth focusing on those that quantify the amount of energy stored in a fixed amount of material. KPIs can be referred to as either the unit of mass of the sorbent (energy storage capacity, ESC) [28] or the unit of volume of the sorbent (energy storage density, ESD) [29,30]. Both KPIs can be used for the characterization of the sorption pair in the laboratory, using the following relationship:

$$ESD = ESC \cdot \rho,$$

where ρ is the mass density of the sorbent. Notably, one material may have a higher ESC value but a lower ESD value than the other, depending on the density of both materials. However, the KPI that should be considered in the selection of materials for thermal storage depends on the application of interest. Mass is important in terms of the cost of the material and weight of the system. However, volume plays a key role when the system needs to be located in a place that is under space constraints or if the cost of containing and maintaining working conditions is high. Thus, it is preferable to have a high mass density, which leads to a low volume, to enhance the value of this KPI. To the best of our knowledge, both KPIs are not always declared in the published literature. Hence, a more comprehensive comparison of the sorbent materials in terms of these two important quantities is desirable.

Charging temperature. During charging, the heat source causes the dissociation of the sorbent and sorbate, which are stored separately until discharging occurs. The required temperature level is an important criterion that indicates which technologies or materials are suitable for a specific situation [27]. As far as solar applications are concerned, collectors may reach up to 150 °C; thus, to adopt them as heat sources in STES, a sorbent material may be selected among those having a charging temperature below 150 °C [24].

Thermal conductivity. The thermal conductivity of the sorbent material is surely an important physical property as it underpins heat transfer within the material. However, the sorbent must also transfer heat with a heat-transfer fluid during both charging and discharging phases. As a result, optimal and efficient heat transport within a sorbent bed is a multifaceted problem affected not only by heat conduction in the material but also by the proper design of the heat exchanger. Furthermore, mass transfer also requires optimization. In the case of solid sorbents, the sorption ability of the material is generally enhanced by maximizing the porosity of the structure, which in turn hinders thermal conduction within the sorption bed. Hence, the requirement for proper heat transfer in STES remains a challenge and it is usually necessary to reach a compromise to ensure good thermal conductivity without limiting other crucial properties[4]. In addition, hydrated salts, which are suitable candidates for sorbents, have intrinsically low thermal conductivities [31]. One possible solution is to add conductive particles, which enhance the thermal conduction of the system [32–36]. However, such measures are relatively rare in existing scientific and technical literature. Lele *et al.* [37] summarized the working principle of the two main methods of thermal-conductivity evaluation: differential scanning calorimetry and radial flow apparatus, called a guarded hot cartridge.

Lifetime. Lifetime (or durability) refers to the number of times the storage unit can release the energy level it was designed for after each recharge and is expressed as the maximum number of cycles [38]. Maximizing the lifetime implies minimizing the deterioration in performance or degradation of the working material with repeated cycling. A long lifetime allows for a reduction in the impact of investment over time. Moreover, as far as the lifetime (expressed in terms of time duration) of such systems is concerned, to our best knowledge, a lack of data can be observed in the current scientific literature. Also on the basis of private communications with relevant industrial stakeholders, and extrapolating from empirical observation on the more mature field of sorption based cooling systems, a reasonable lifetime of 20 years of well-maintained thermochemical energy storage systems can be envisioned.

Cost and Availability. The availability and commercial price are mandatory considerations when evaluating the feasibility and scalability of a system. Highly performant but expensive materials do not offer a reliable solution for TES[39].

Other economic-social KPIs are related to investment, operational, and maintenance costs, which are related to the type of plant. In addition, other KPIs focus on environmental issues, such as health and sustainability risks. In this review, these KPIs will not be considered, but they can be analyzed from existing literature [27].

3. Classification of sorbents

Yu *et al.* [40] proposed a classification of sorption materials for TES and distinguished between four different categories: liquid absorption, solid adsorption, chemical reaction, and composite material. Typical parameters for each class are listed in Table 1.

3.1 Liquid absorption

In the case of liquids, the physical mechanism behind the process is the absorption of a fluid (solvent) into a liquid (solute), thereby forming a solution with a concentration that changes during the entire cycle. In particular, the temperature of the solution changes with the concentration under a fixed sorbate vapor pressure. A comprehensive analysis of the liquid adsorption solution was performed by Hui *et al.* [13], who compared the working behaviors of seven absorption couples: $CaCl_2/H_2O$, glycerin/H_2O, KOH/H_2O, LiBr/H_2O, LiCl/H_2O, NaOH/H_2O, and H_2O/NH_3.

Table 1: Typical charging temperature and ESD values of the four categories of sorbent materials: solids, liquids, chemicals, and composite materials.

Category	Charging temperature [°C]	Energy storage density [MJ kg^{-1}]
Liquid	40-150	190-4400
Solid	90-160	35-950
Salt	50-190	1500-2240
Composite	75-150	340-2800

The thermodynamic cycle in the case of seasonal storage is similar to that shown in **Figure 8**. This can be briefly described as follows. During the summer, a solution with a low mass fraction of absorbent (*poor solution*) flows from the solution tank to the generator, where it can be heated using solar energy. Upon heating, the sorbate is vaporized and transferred to the condenser, where it condenses and releases latent heat. The latter can be released or, sometimes, exploited to heat water. Sorbate, in condensed form, is stored in the sorbate tank. The remaining solution (*rich solution*), which is characterized by a high mass fraction of absorbent after the desorption of the sorbate, flows back to the solution tank. During winter, the sorbate evaporates and, following the solution thermodynamic equilibrium, is absorbed by the rich solution. During absorption, heat (Q_{abs}) is released and used to fulfill the energy requirements for space heating. The cycle ends with the return of the poor solution to the solution tank. Depending on the configuration of the system and the absorbate-absorbent nature, the liquid solution can reach its crystallization point. As an example, **Figure 9** shows the seasonal solar energy storage cycle of LiBr/H_2O. If crystallization is avoided, the pressure of the solution P(T) follows the blue line, and the main steps are as follows:

1→ 2: poor solution is heated by the energy source (e.g., solar energy), keeping the absorbent concentration constant;

2→ 3: the solution is heated and the absorbate is desorbed from the solution, following the solution thermodynamic equilibrium C; the desorbed absorbate condenses

3→ 5: during storage (heat preservation), the solution at state 3 is cooled to state 5 at the temperature of the outdoor environment;

5→ 6: the solution absorbs vapor from the evaporator, the mass fraction of the solution decreases, and its pressure increases until it is equal to that of the evaporation (point E)

6→ 7: heat can be used for space heating, and the solution leaves the absorber after the absorption

7→ 1: the solution goes back to the solution storage tank

If crystallization is not avoided, P(T) follows the additional orange path. The mass fraction of the absorbent at 3' is higher than that at 3. During storage, P(T) crosses the crystallization line in state 4, and crystals appear in the solution tank and grow until state 5. Notably, the presence of crystals requires higher system complexity. However, this may reduce the volume of the material and the cost of the system.
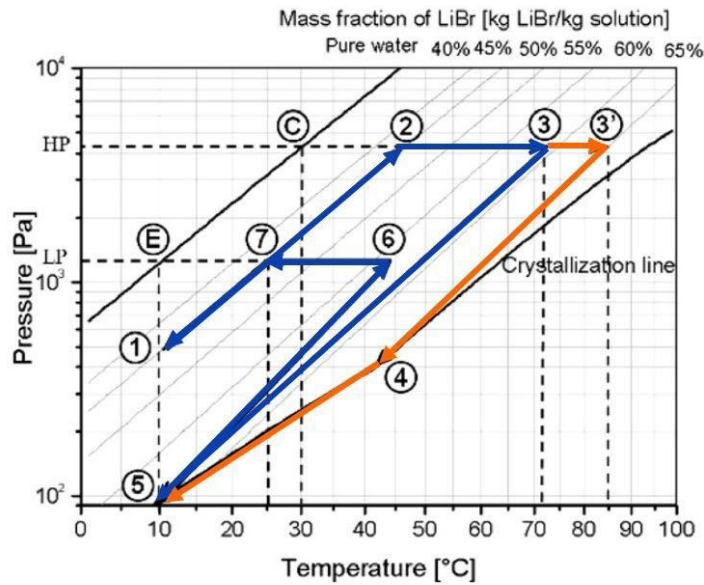

Figure 9: Thermodynamic cycle of a seasonal solar energy storage plant adopting LiBr/H$_2$O working pair [13]. See text for details.

Generally, the heat transferred from state *i* to state *j* can be calculated by the energy balance equation, without considering the power required to operate the pumps:

$$Q_i = m_j h_j + m_{vap,i} h_{vap,i} - m_i h_i, \qquad (1.1)$$

where h$_{vap,i \to j}$ is the enthalpy of evaporation of the absorbate that is evaporated from the solution [13]. The solar energy required for dehydration is Q$_{1\to3}$ or Q$_{1\to3'}$, and the heat of absorption corresponds to Q$_{5\to7}$. Some considerations must be taken when choosing the proper absorbent-absorbate couple. First, the selected couple may present a large amount of Q$_{abs}$, thereby offering high ESD or ESC values. Moreover, as already mentioned, the temperature of desorption of the absorbate from the absorbent may be minimized. This enables the proper functioning of the system, even at low temperatures, that is, the amount of thermal energy to be collected to promote the charging step is minimized. Moreover, the efficiency of the solar collectors decreases with the temperature difference between the liquid in the collector and the ambient environment because the thermal losses increase. During charging, the solution is heated, and the absorbate is desorbed from the solution following the thermodynamic equilibrium of the solution at the condensation temperature Tc. Hence, a second requirement for the choice of the absorption couple is to minimize the condensation temperature Tc. Finally, as shown in a typical P(T) chart, the absorption temperature increases with increasing evaporation temperature, which becomes an additional criterion for the selection of the absorbent-

absorbate couple. However, decreasing the condensation temperature while increasing the evaporation temperature is difficult because they typically follow similar trends. Generally, the higher the absorption temperature, the higher the heat required from the collectors. Therefore, the choice of sorption couple requires a compromise between the two. Moreover, safety parameters (toxicity, flammability, and reactivity) and low investment costs should be considered. Examples of liquids typically used for STES with the corresponding relevant figures are reported in Table 2.

Table 2: Typical liquid sorbent materials for STES systems and corresponding figures and values

Material	Price [€/ton]	Tc [°C]	Td [°C]	Additional information	Water uptake [g/g]	ESD [MJ/m^3]	ESC [kJ/kg]	SCC [€/kWh]	Ref.
$CaCl_2/H_2O$	160	44,8	20-45	Tcond=30 °C, Tev=10 °C	0,398	429	914,00	0,6297	[13]
$Glycerin/H_2O$		53		Pads=1.2 kPa, Pdes=5.6 kPa	0,9	180	193		[13]
H_2O/NH_3		155,5			0,9	352	1317,00		[13]
KOH/H_2O	1200	63			0,508	1125	2618	1,6488	[13]
$LiBr/H_2O$	5500	72			0,588	1125	2019,00	9,7990	[13]
$LiCl/H_2O$	2700	65,6			0,443	1440	4387,00	2,2139	[13]
$NaOH/H_2O$	400	50			0,335	554,4	1558,00	0,9235	[13]

3.2 Solid adsorption

Solid systems are based on adsorption, that is, the interaction between the surface of a solid (*adsorbent* or *sorbent*) and the molecules of a fluid (*adsorbate* or *sorbate*) (**Figure 10**). The adsorption mechanism is driven by an imbalance of forces experienced by surface atoms that cannot completely saturate their bonds. Depending on the nature of the gaseous molecules and solid surface, two types of adsorption may occur: physical or chemical. *Physisorption* is based on weak van der Waals forces, and it generates a relatively low adsorption heat (lower than 80 kJ per mol of sorbate [41–43]).

This phenomenon does not require any activation energy and is generally easy to reverse by simply applying heat and/or a vacuum. This can be irreversible in the case of capillary condensation. When the adsorbent has a porous structure, the pore spaces are filled with condensed liquid. Owing to an increase in the number of van der Waals interactions between vapor-phase molecules inside the confined space of a capillary, condensation can occur below the saturation vapor pressure.
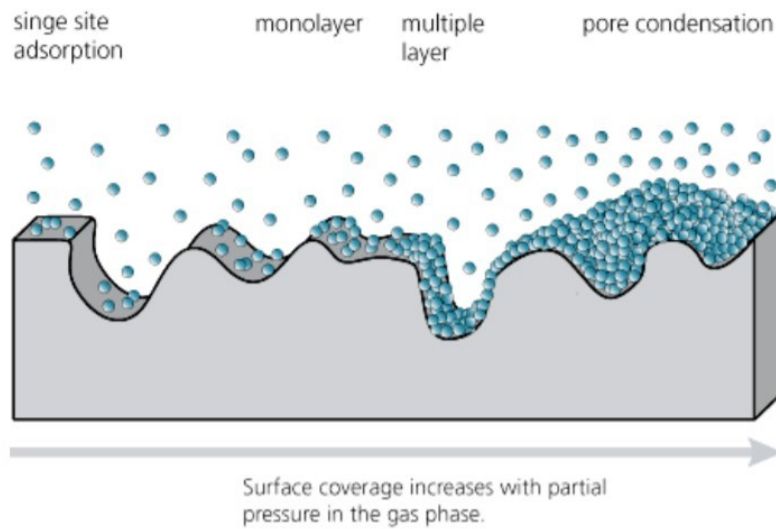
singe site
adsorption

monolayer multiple
layer

pore condensation

Surface coverage increases with partial
pressure in the gas phase.

Figure 10: Pictorial representation of the mechanism of adsorption, with the formation of the monolayer, multilayer, and pore condensation.

Therefore, lower pressures are required to remove the sorbate during desorption. In most cases, low-temperature heat-storage systems exploit the physical sorption of porous solid materials. The capacity of a solid for fluid adsorption depends on its pore system geometry and the chemical properties that define the fluid-solid interaction [44]. If chemical bonds are involved, this phenomenon is defined as *chemisorption*. It is accompanied by a considerably higher energy, which depends on the nature and strength of the chemical bond between the adsorbent and adsorbate. The main factors that determine the amount of the sorbate that is adsorbed on the surface of the adsorbent at equilibrium are temperature, pressure, and specific surface area (SSA) of the solid. In the case of chemisorption, in which the development of chemical bonds between the adsorbent and adsorbate requires direct contact between the two phases, only a single layer of gaseous molecules can be formed on the free solid surface. Therefore, the number of adsorbed molecules is directly proportional to the SSA. In contrast, in the case of physisorption, gaseous molecules can overlap with others, forming a multilayer structure [45]. Thus, the extension of the SSA increases from nonporous materials to microporous materials. It should be noted that microporous materials are at risk of the size-exclusion effect, where only small particles pass through the pore structure [46]. However, this must be considered only in the case of competition between different-sized molecules. Alternatively, the microporous structure may not undergo capillary condensation (typical of mesopores), which causes an increase in the mass-transfer resistance. Adsorption is typically represented by isotherm, isobar, or isostere curves. Representative examples are shown in **Figure 11**.
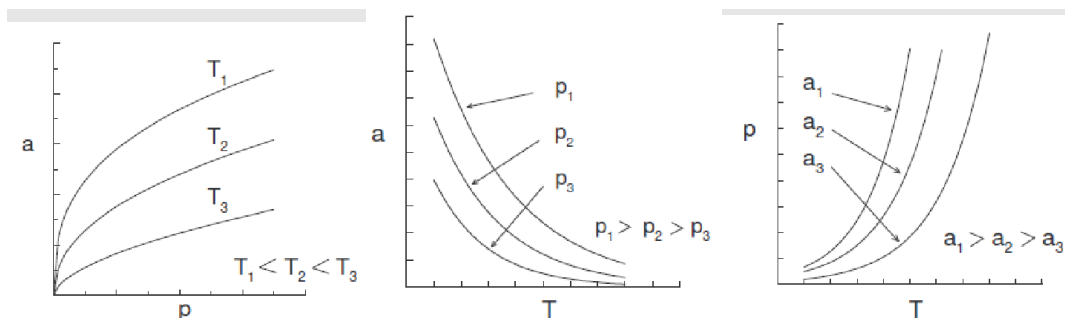

Figure 11: Ideal representation of isotherm, isobar, and isostere curves [47]

The study of the adsorption of gas molecules on a porous solid surface is generally conducted using Brunauer–Emmett–Teller theory [48], which is also the basis for the analysis of SSA measurements [49]. This theory suggests that the adsorbed gas quantity (for example, in terms of volume) can be plotted with respect to its pressure. Using this principle, five curve categories can be classified according to the morphology of the porous structure (**Figure 12**).

Curve I (also referred to as Langmuir type [43]) is typical for cases where only a single layer of gas molecules is formed directly in contact with the surface. Here, the curve presents a steep initial portion, which approaches the limiting adsorption saturation loading at a medium relative pressure (P/P_0). Adsorbents displaying this type of isotherm present a high affinity with gaseous molecules. Hence, the adsorption occurs fast, but it is limited by the complete coverage of the solid surface. Therefore, the saturation value is controlled by the accessible pore volume.

For curves II, III, IV, and V, the adsorption phenomenon is not limited by monolayer formation. Curve II is typical for nonporous or macroporous materials. Curve III exhibits reversible adsorption, which occurs when the adsorbate-adsorbate interactions are stronger than adsorbate-adsorbent interactions. Curve IV describes capillary condensation, where the last part of the curve is related to condensation in micropores (diameter > 20 A) before it reaches the saturation pressure [50,51]. The isotherm shape of curve V is similar to that of curve III, which can be attributed to relatively weak adsorbent–adsorbate interactions [52].
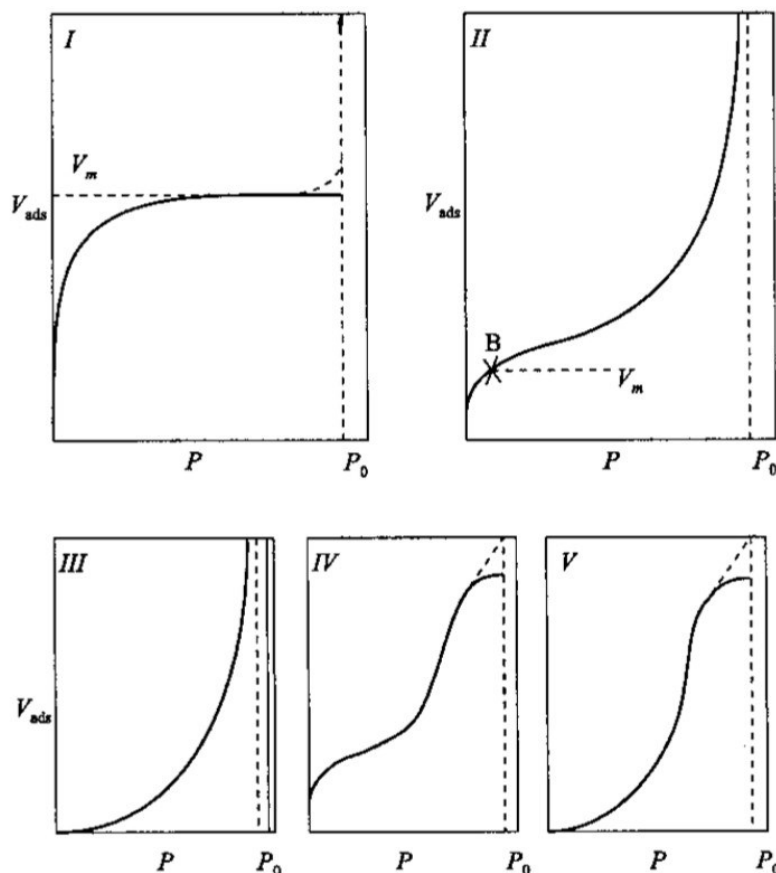
Figure 12: Schematic of different curves based on the morphology of the solid structure [52]

The characteristics of an ideal adsorbent strongly depend on the requirements of the process (i.e., charging or discharging temperature); therefore, there is no general adsorbent for heat-transformation applications. Hence, extensive research has been conducted on the development and testing of novel adsorbents; these studies attempt to determine the relationship between the adsorbent structure and

sorption properties. The most important figures of merit for a given adsorption material for heat-transformation applications are the load span (i.e., the difference in sorbate uptake between the charged and discharged states) and isosteric heat, which is typically expressed with regard to one mole of sorbate (kJ/mol). Additional consideration must be given when screening different porous sorbents with regard to hydrophilic or hydrophobic behavior [53]. Hydrophilic typically refers to a high affinity for water. However, in the case of porous materials, water adsorption loading is dictated by the pore volume. Hence, the hydrophilicity of a solid adsorbent is determined by the selectivity of the material toward water over other components in a mixture. The most commonly employed solid materials for thermal storage are silica gel, zeolite, activated carbon, natural rock, and novel porous solids, such as aluminophosphate (AlPO), silico-aluminophosphate (SAPO), and metal–organic frameworks (MOFs) [53]. Silica gel, which is a highly porous, non-crystalline form of silica, is suitable for low-cost and low-temperature heat-storage applications, owing to its low regeneration temperature from 50 °C to 90 °C [54]. Porous silica gel consists of an incompletely dehydrated polymeric structure of colloidal silicic acid, which has the formula $SiO_2 \cdot *nH_2O$. Its surface is primarily composed of Si-OH and Si-O-Si groups [55]. Water molecules can be adsorbed on silanol groups through hydrogen bonding or physically adsorbed by hydrogen bonding between water molecules to form H_2O clusters and possibly water condensation on top of these groups (**Figure 13**).

Modeling the interaction between water and the silica surface was proposed by Fang *et al*. [56]; at relatively low temperatures (approximately below 160 °C), only physical desorption occurs. The desorption of H_2O bonded to -OH groups requires high temperatures of up to 400 °C. Because the desorption temperature in the adsorption-desorption cycle for thermal storage in civil applications does not exceed 150 °C, chemical bonds are not involved. Consequently, the amount of energy associated with the sorption phenomenon is relatively low (typically does not exceed 25 kWh/m³). In addition, Chang *et al*. [57] investigated the effect of the regeneration time and temperature on moisture adsorption in packed silica gel beds and observed that the amount of adsorbent increased with the degree of regeneration. The study highlighted the advantage of using modified silica gel, which has a microporous structure, as opposed to commercial silica gel, which generally presents a mesoporous structure, owing to the low mass-transfer resistance of the former. The mesoporous structure is affected by capillary condensation, which causes hysteresis (i.e., kinetic slowing) in the adsorption-desorption cycle.
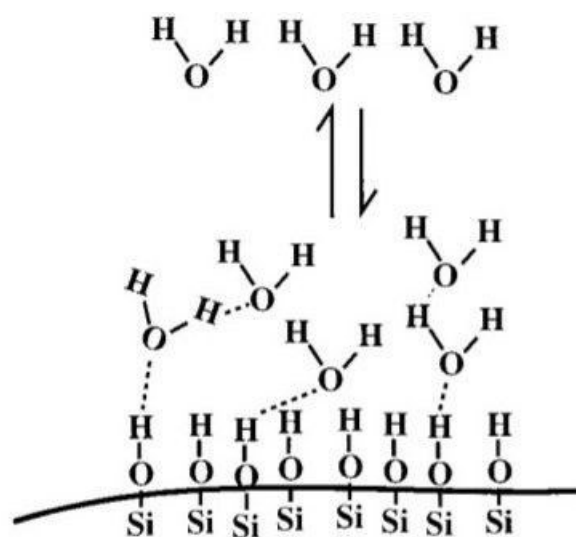

Figure 13: Schematic of the water adsorption mechanism upon a silica surface [56].

Zeolites are crystalline hydrated aluminosilicates with small pores that are comparable to those of molecules in frameworks based on extensive three-dimensional (3D) networks of oxygen ions [58].

The large energy sorption density and capacity are due to the higher strength of the sorbent–sorbate bonds that characterize the zeolite mechanism of adsorption. In addition to the morphology of the porous structure (size, SSA, and pore volume), its adsorption ability is strictly related to the Si/Al ratio [59]. Materials with low Al content per unit cell are characterized as hydrophobic. This is owing to the low concentration of hydrophilic protons in the material and the weak interactions between Si-O-Si and oxygen [60]. However, stronger hydrophilic behavior does not always result in higher adsorption performance. Henninger *et al.* [61] performed molecular simulations of water adsorption in various zeolites to understand the fundamental relationship between the adsorbent microstructure and water adsorption equilibrium, with particular regard to the Si/Al ratio. By comparing Li-Y zeolites with Si/Al with ratios of 2.5, 7, and 11, relative water uptakes (i.e. difference in water amount between adsorption and desorption stages) of 0.24 g/g, 0.34 g/g, and 0.37 g/g were observed, respectively. Higher loading lift values with higher Si/Al ratios are due to the lower water loadings at the charging temperature; this occurs due to the lower hydrophilicity of the structures with less Al. An analysis of zeolite Na-A showed a decrease in water uptake at 150 °C, from 0.229 to 0.09, when Si/Al changed from 2.49 to 10.29. In addition, this study presented significant differences between the simulated and experimental data. This may be due to post-synthetic treatments, which seem to cause partial destruction of the pore structure, as reported in Refs. [62,63]. The latter phenomenon can cause a reduction in the water adsorption capacity in relation to the simulation results because the framework is free of crystal defects. The adsorption heat increases when small cations (e.g., $Na^+ Li^+$) are introduced into the zeolite structure. Jentys *et al.* [64] analyzed the surface chemistry of water adsorbed on zeolites and a series of alkali-metal zeolites through transmission absorption infrared spectroscopy. For traditional zeolite, the shape of the adsorption isotherm of water is of type "I." This reflects the tendency of the material to exhibit preferential water clustering (i.e., interactions between adsorptive molecules). Thus, the interactions among water molecules are of a higher strength than that of a second water molecule with the adsorption site, thereby resulting in a physisorption mechanism (**Figure 14**). This situation is more complicated with alkali-metal-exchanged zirconia. At low pressures, the presence of alkali metal cations prevents the clustering of water molecules; therefore, all water molecules are bound to the cations on the solid surface.

The interaction of the second, third, or fourth water molecule with the alkali-metal cation is stronger than that among the water molecules themselves; therefore, chemisorption is favored over physisorption (**Figure 15**). As a result, the adsorption ability increases. Finally, at higher equilibrium pressures, a second water shell starts to form. Jänchen *et al.* [65] investigated and confirmed an improvement in the storage properties via ion exchange using physico-chemical methods such as thermogravimetry, differential scanning calorimetry, microcalorimetry, and isotherm measurements. In their study, selected materials were pelleted and tested in lab-scale storage; the ESC results were 536 kJ/kg for Zeo-NaX and 630 kJ/kg for Zeo-MgNaX. Notably, the high strength of sorbate-sorbent bonds causes a high regeneration temperature. For Zeo-NaX and Zeo-MgNaX, a charging temperature of 180 °C was necessary. Hence, when modifying the chemical structure of a zeolite, a compromise between the water sorption capacity and regeneration temperature is mandatory.

A system for energy storage using 7000 kg zeolite 13X was installed in a school building in Munich, Germany in 1996 and connected to the district heating system; an energy density of 124 kWh/m^3 was experimentally obtained [66]. The Institute for Thermodynamics and Thermal Engineering (ITW), University of Stuttgart, investigated chemical heat-storage technologies for low-temperature applications through a laboratory test rig, and the ESD and ESC results were 450 MJ/m^3 (643 kJ/kg) and 353 MJ/m^3 (504 kJ/kg) for zeolite 4A at charging temperatures of 180 °C and 150 °C, respectively [67]. More recently, Wu *et al.* [68] tested the potential use of commercially available 13X zeolite,

modified by an ion exchange with cerium-compensating cations, for the low-temperature storage of solar energy. Moreover, Monte Carlo simulations were used to determine the limiting values of the amount of adsorbed water vapor and the differential heat of adsorption, which can be obtained experimentally if the zeolite samples are completely dried. An investigation of the stability of the zeolite structure showed energy storage capacity losses of 25% and 36% for zeolite and Ce-exchanged zeolite, respectively (from 800 kJ/kg to 600 kJ/kg and from 1100 kJ/kg to 700 kJ/kg, respectively), which proves that zeolites require higher charging temperatures to completely desorb water.
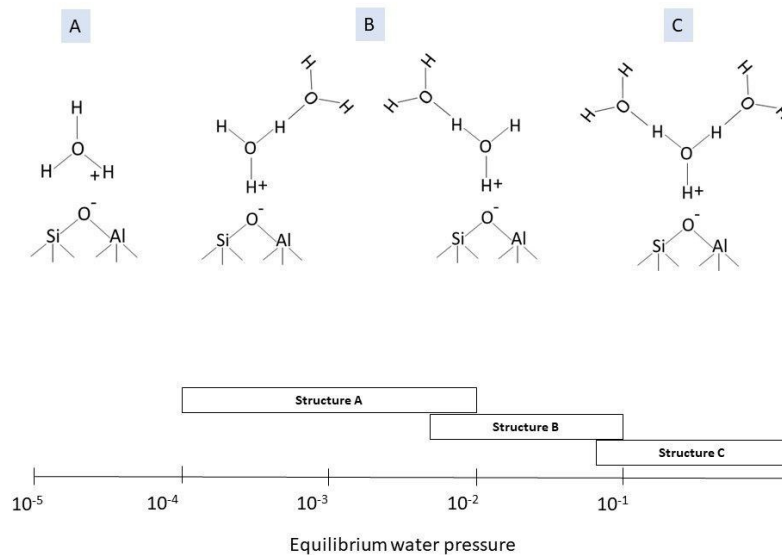
Figure 14: Schematic of the mechanism of adsorption on the surface of a zeolite. Image adapted from [64].
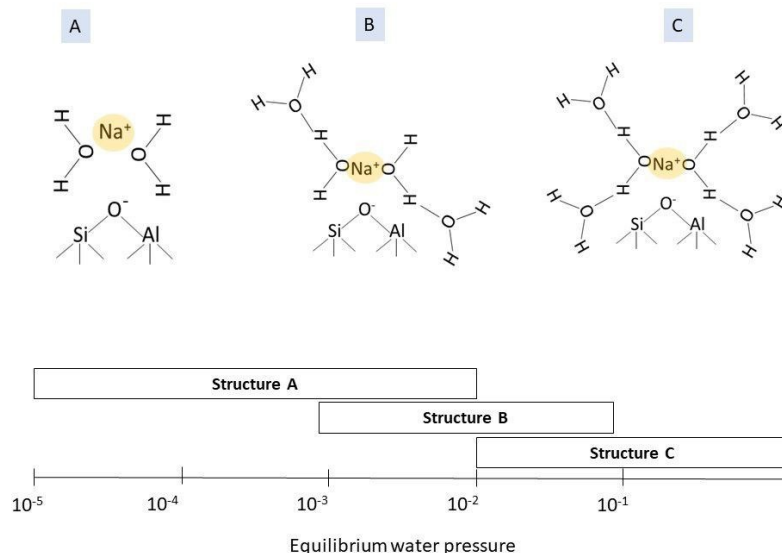
Figure 15: Schematic of the mechanism of adsorption on the surface of a zeolite in the presence of cations. Image adapted from [64].

AlPOs are isoelectronic analogs of silica-zeolites, which were first reported by Wilson *et al.* in 1982 [69]. The basic building units are composed of AlO_2^- and PO_2^+, which form $AlPO4$. They are alternatively distributed, thereby generating a neutral 3D-framework with well-defined channels or cavities of the size of small molecules [70]. AlPO molecular sieves cover a wide range of different

structure types, which are denoted with a number "*n*" following the acronym AlPO. Several databases, such as [71], list all the possible structures. It is possible to introduce new atomic elements into the structure of AlPOs. For example, SAPOs were synthesized by substituting Si atoms with P atoms. Si atoms can replace P atoms at isolated tetrahedral sites, or they may aggregate in large assemblies to form Si islands. This substitution introduces Brønsted acids (i.e., species capable of donating a proton) into AlPO-based molecular sieves. Owing to the potential use of AlPOs and SAPOs in heat-transformation applications, several studies have investigated the adsorption of water in these systems [42,72]. Interestingly, those materials exhibit S-shaped water adsorption isotherms and isobars—a feature that is attractive because a large amount of sorbate can be reached via a moderate change in pressure and temperature. The sigmoidal shape of an adsorption isotherm is generally caused by lateral attractive interactions between the adsorbed species[73]. This is identical to the type V IUPAC classification [73]. In particular, Henninger *et al.* [61] reported that compared to traditional zeolites, AlPOs exhibit a step-gradient of relative water uptake in a narrow temperature range, and they provide more advantages for thermal storage applications than the larger isobars of classical zeolites (**Figure 16**). The energy analysis performed by Poulet *et al.* [74] showed that the stability of the AlPO34 hydrated structure was not induced by the individual interaction of water molecules with the AlPO4 channel, but via the formation of a collective hydrogen-bond network. This explains why the system exhibits an abrupt transition between an empty and full phase with 12 water molecules per unit cell. Through comparative thermogravimetric and calorimetric studies, Ristic *et al.* [75] highlighted the performance of different microporous AlPOs and correlated the results with their structural features. They explored the role of pore morphology and identified that regular elliptical cages ensure lower relative pressures for water adsorption than elliptical, pear-shaped pores. The presence of dopants in AlPOs, which result in SAPO molecular sieves, appears to enhance the water sorption capacity because structural defects enable better interactions between polar water molecules and the surface. In particular, gradual water uptake is governed by the presence of randomly distributed Si in the framework. Si^{4+} atoms typically replace P^{5+} in the AlPO structure. This leads to the formation of highly acidic bridging OH groups (Si-OH-Al), which are the primary sites for adsorption [75]. However, it is difficult to determine which material has the best sorption capacity between AlPOs and SAPOs. Several studies have identified the thermal instability of SAPO materials, which makes them less attractive for STES systems, where reasonable cyclability is desirable. Ristic *et al*. [75] reported the significant hydrolysis of SAPO-34 in water and the formation of an amorphous phase after six months. In addition, they emphasized the transfer from the framework acidic -OH group to water with the formation of H_3O^+. SAPO-34 requires a charging temperature of 140 °C, whereas AlPO zeolites exhibit good performance with a charging temperature of 95 °C. Baver *et al.* [76] studied the stability of AlPO and SAPO zeolites through *in situ* X-ray diffraction measurements. They observed that the incorporation of silicon and, hence, the hydrophilicity of SAPO34 are crucial for stability. High silicon content (e.g., SAPOs) causes fast irreversible structural degradation, whereas low silicon content (e.g., AlPOs) causes complete reversible structural changes, thereby ensuring structural integrity. Notably, the thermal degradation of SAPO34 is well known, and several studies have been conducted in this field. Henninger *et al.* experimentally demonstrated that water adsorption properties strongly depend on sample preparation. SAPO34 synthesis using morpholine as a template exhibited material degradation after some cycles. As a result, SAPO34 was observed to have a high load and good stability or a loss of 25% over six cycles, depending on the method of preparation, as shown in **Figure 17** [77]. However, older studies have demonstrated that SAPO34 is affected by the loss of crystallinity during water adsorption [78,79]. Samples containing Si islands can restore their crystallinity after prolonged exposure to humidity, whereas samples with isolated Si lose their crystallinity irreversibly, owing to the increased likelihood of the hydrolysis of Si-O-Al linkages [80,81]. Recently, Fischer *et al.* [82] studied the interaction of different SAPO34

models with water using dispersion-corrected density functional theory (DFT-D) calculations. It was observed that synthesis routes or post-synthesis treatments (leading to the formation of Si islands) must be favored when targeting SAPO34 as an adsorption material, owing to the positive influence of Si islands on the material stability. Finally, they presented the negative influence of defects on the structure, thereby confirming the crucial role of the SAPO-atom structure in the definition of its performance in relation with AlPO molecular sieves.
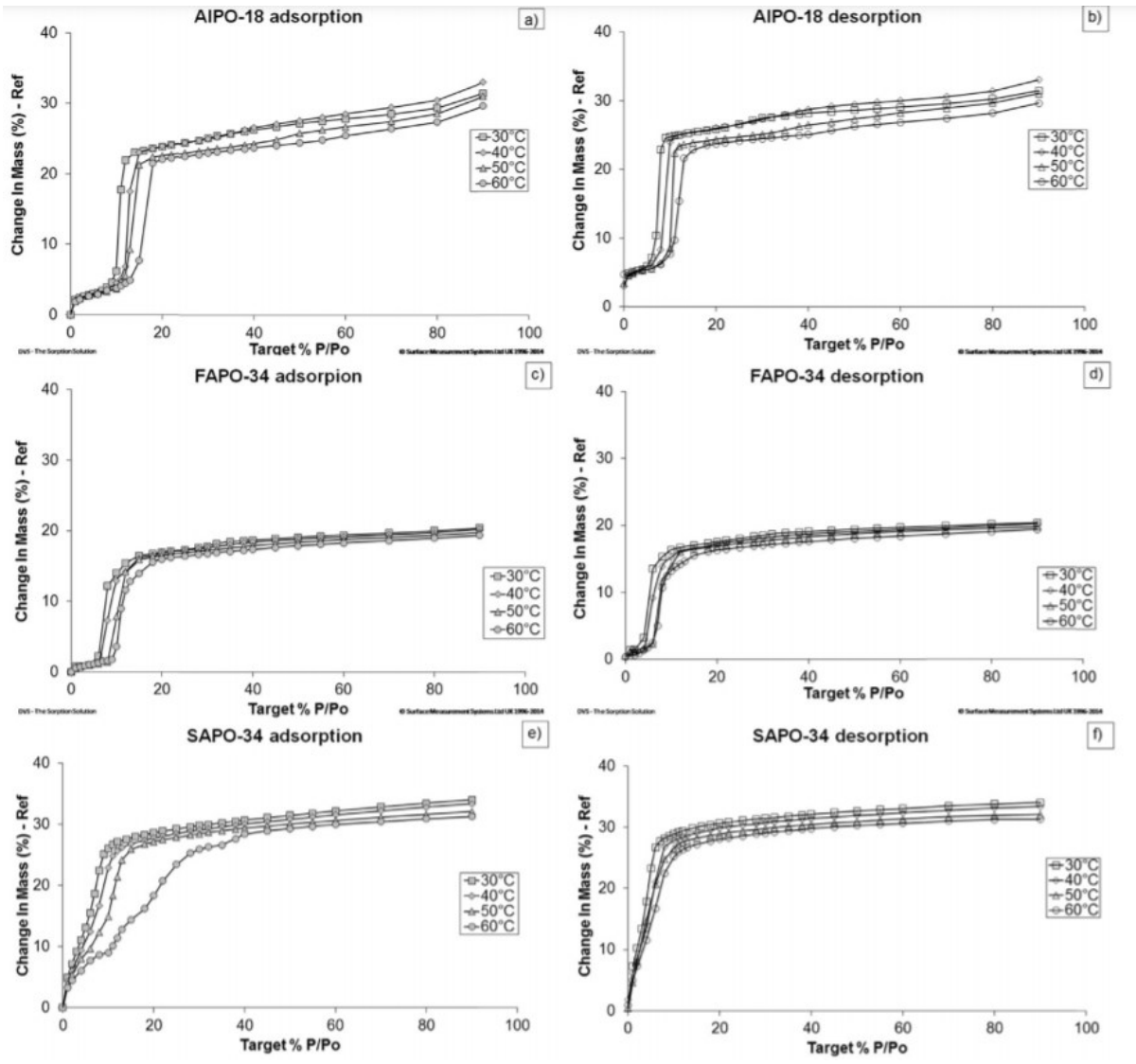

Figure 16: Adsorption/desorption isotherms at 30 °C, 40 °C, 50 °C, and 60 °C measured for adsorbent materials: a-b) AlPO-18; c-d) FAPO-34; e-f) SAPO-34 [83]
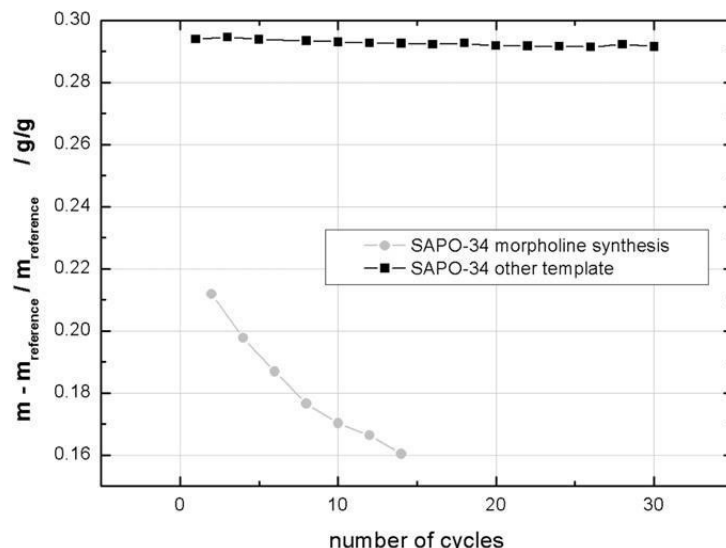
Figure 17: Material degradation with the number of cycles in SAPO-34 [84]

MOFs are organic-inorganic hybrid crystalline porous materials consisting of a regular array of positively charged metal ions surrounded by organic "linker" molecules. The metal ions (typically named inorganic secondary building units) form nodes that bind the arms of the linkers (typically called organic secondary building units) together to form a repetitive cage-like structure (**Figure 18**). Different metal centers and ligands can be selected to produce MOFs as molecular building blocks; therefore, high flexibility is possible when modifying physical and chemical features [85,86]. MOFs have an extraordinarily large internal surface area, large pore volume, and variable pore size, owing to their hollow structure [87]. Various types of MOFs have been synthesized. Adsorption occurs on metallic clusters according to the structure, which modifies the first coordination sphere of the metal ion (chemisorption) or layer/cluster (reversible) adsorption. Owing to the large number of combinations of inorganic clusters and organic ligands, approximately 20,000 different MOFs have been synthesized [88]. MOFs differ from each other by characteristics, such as the specific surface chemistry or metal-cluster family, which in turn can define the way MOFs interact with specific molecules (i.e., their hydrophilic or hydrophobic character) or their physicochemical stability. For clarification, Peyman *et al*. [89] divided the overarching family of MOFs into a number of subgroups according to their key chemical and physical features, such as metal clusters, network and pore dimensionality, and surface chemistry. The presence of unsaturated metal centers plays a crucial role in ensuring the good adsorption ability of MOFs because they offer extra binding sites to the guests to capture water. When water enters the MOF structure, the metal clusters first coordinate water molecules before capillary condensation of water occurs in the pores [90]. Most MOFs present a type-I isotherm, which has good affinity with the adsorbate. However, other types of adsorption isotherms also exist. Examples of different isotherm water adsorption curves are shown in **Figure 19**, with relative considerations to the water physisorption properties of MOFs [90–92]. Among MOFs, the most widely studied materials for STES are MIL100(M^{3+}), where M^{3+} is typically Fe^{3+}, Al^{3+}, or Cr^{3+}. These consist of a 3D system of mesopores that are formed from the octahedra of M^{3+} trimers connected by oxygen atoms from the BTC (benzene-1,3,5-tricarboxylic acid) ligand. They can present both micropores (<8 nm) and mesopores (<30 nm) [93]. The main advantage of MIL100(M^{3+}) is the presence of highly charged M^{3+}, which are used to assemble the structure. They form a strong metal-ligand bond, which results in excellent stability. The water sensitivity of some MOFs has been well documented, and the thermal cycling stability is widely considered to be a challenge. Numerous studies are dedicated to the analysis and review of MOF stability [93–95].
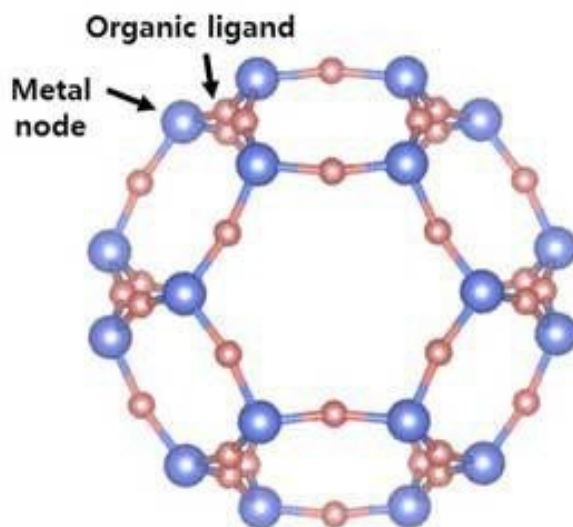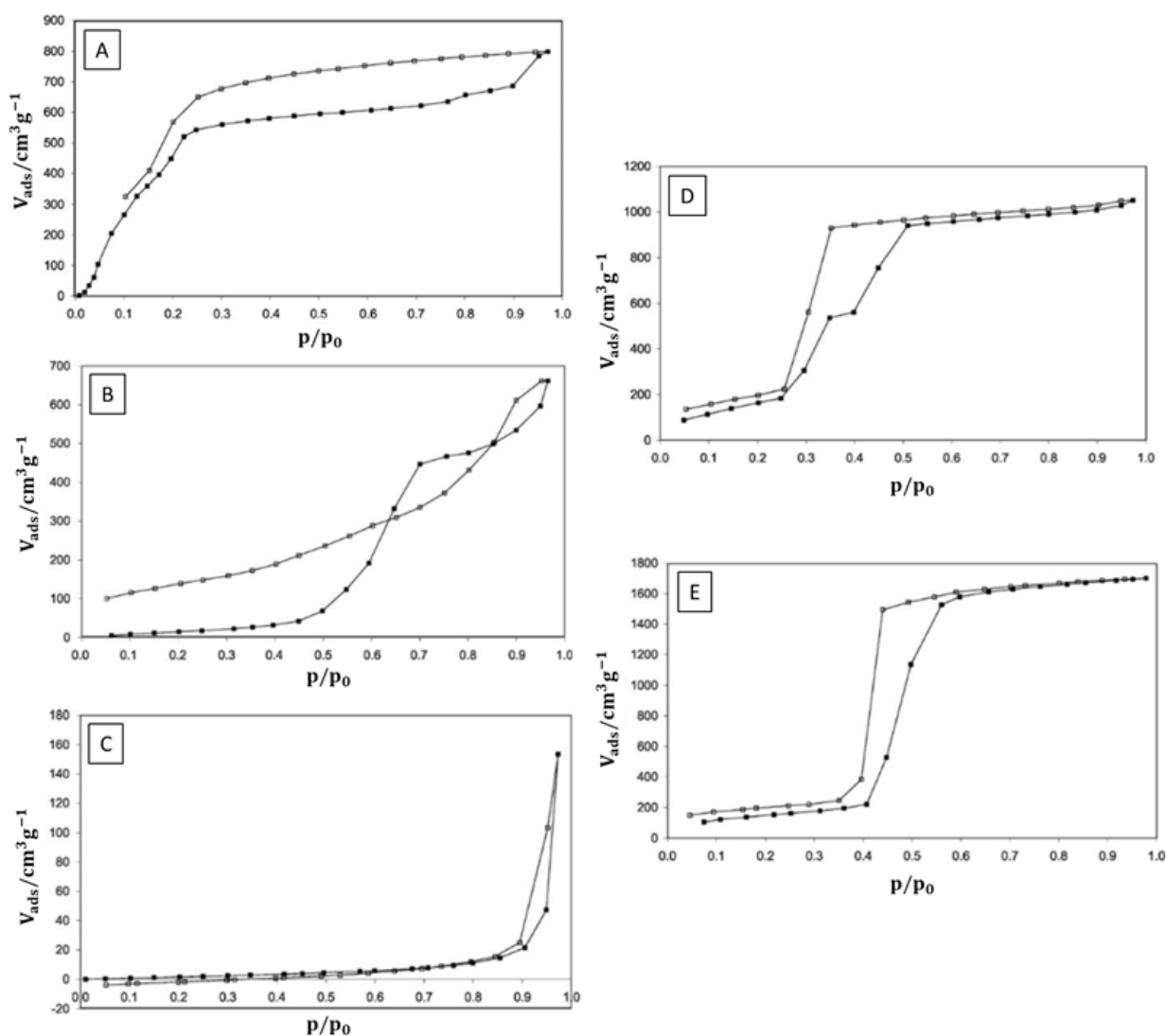
Figure 18: Schematic of the MOF structure

Figure 19: Water adsorption (solid symbols) and desorption (open symbols) isotherms of (a) DUT-4, (b) ZIF-8, (c) H-KUST-1, (d) MIL100(Fe), and (e) MIL101 [91]

In addition to the four classes of adsorbents discussed previously, other materials have been studied for water adsorption, and *activated alumina* (AA) is a popular alternative. Carruthers *et al.* [96] proposed five mechanisms for AA-water adsorption:

i) hydrogen bonding between water molecules and the surface hydroxyl group;

ii) hydration of cations on the surface;

iii) dissociative chemisorption (in the case of alpha alumina);

iv) deep hydration of poorly ordered Al^{3+}, originally solvated, and not fully coordinated in the ordered structure;

v) hydroxide or oxide-hydroxide formation in depth.

Chemisorption is generally not involved when such material is used for STES; therefore, a relatively low regeneration temperature is required. Hua *et al.* [97] reported an experimental energy density of 38.30 kWh/m^3 with inlet air of RH=50% and a regeneration temperature of 120 °C.

Clays, which are chemically inert, resistant to deterioration, and commercially available in large quantities and usually low cost, have been investigated as adsorbents. The atomic structure of clay minerals consists of two basic units: an octahedral sheet and a tetrahedral sheet. The octahedral sheet consists of closely packed oxygen and hydroxyl molecules, in which Al is arranged in octahedral coordination. The second unit is the silica tetrahedral layer, wherein the silicon atom is equidistant from four oxygen or possibly hydroxyl molecules, thereby forming a tetrahedron with Si at the center. Montmorillonite, which belongs to the family of clays, consists of one alumina octahedral sheet sandwiched between two silica tetrahedron sheets [98]. The substitution of Fe^{2+} and Mg^{2+} atoms for Al^{3+} in the octahedral layer imparts a net negative charge to the overall structure. Consequently, exchangeable cations (e.g., Na^+, K^+, Ca^{2+}, or Mg^{2+}) are introduced into the interlayer space to compensate for the negative charge [99].

When exposed to water, montmorillonite clay can absorb large quantities of water, up to 10 times its volume. The adsorption energy of water is the driving force against the electrostatic attraction between the negative layers and cations and the van der Waals attraction between the layers.

The hydration–dehydration behavior of bentonite, an absorbent aluminum silicate clay primarily consisting of montmorillonite, has been widely studied for STES [100,101]. Salles *et al.* [102] reported that the driving force for the hydration of montmorillonite-type clays is generally a function of the nature of the interlayer cation (Na^+, Ca^{2+}), its charge, and its size. However, it must be noted that it is challenging for bentonite to adsorb large amounts of water. Jabbari *et al.* [103] reported that pure bentonite adsorbs more water than silica gel and alumina at RH = 30%. Their study shows that this behavior may be related to the non-rigid structure of bentonite, which can host large quantities of water by swelling. Even if this results in a higher quantity of heat during adsorption, swelling is an undesirable phenomenon that negatively affects the system. Olphen *et al.* [104] investigated the adsorption-desorption behavior of vermiculite clays. The adsorption of water appears to occur in two distinct steps that correspond to the intercalation of the lattice with one and two monomolecular layers of water, respectively. The observed hysteresis of the isotherm may be due to the retardation of the adsorption process, owing to the development of elastic stresses in the crystalline structure during the first penetration of water between the unit layers. However, the heat of the hydration of clays is relatively low while the pore volume is large; therefore, bentonite and vermiculite are typically used as porous hosts for hygroscopic salts. Examples of the main solid materials used for STES are shown

in Table 3 and **Figure 20**, and their commercial prices are listed in Table 4. In Table 5 important physical properties for some of the most popular commercial sorbent materials are also reported.

Notably, the reported values were obtained through isosteric or calorimetric methods or through open or closed systems. To properly compare different materials, it is important to be aware of the energetic losses that affect the sorption cycle of a system (pressure or thermal losses). These losses are specific to each method that is used to evaluate material performance. Therefore, knowledge of the method that was used provides access to a more complete comparison of the adsorbents. Additional information and references are given in Table 3 at the end of the report. Water was the sorbate for each adsorbent material, unless stated otherwise.
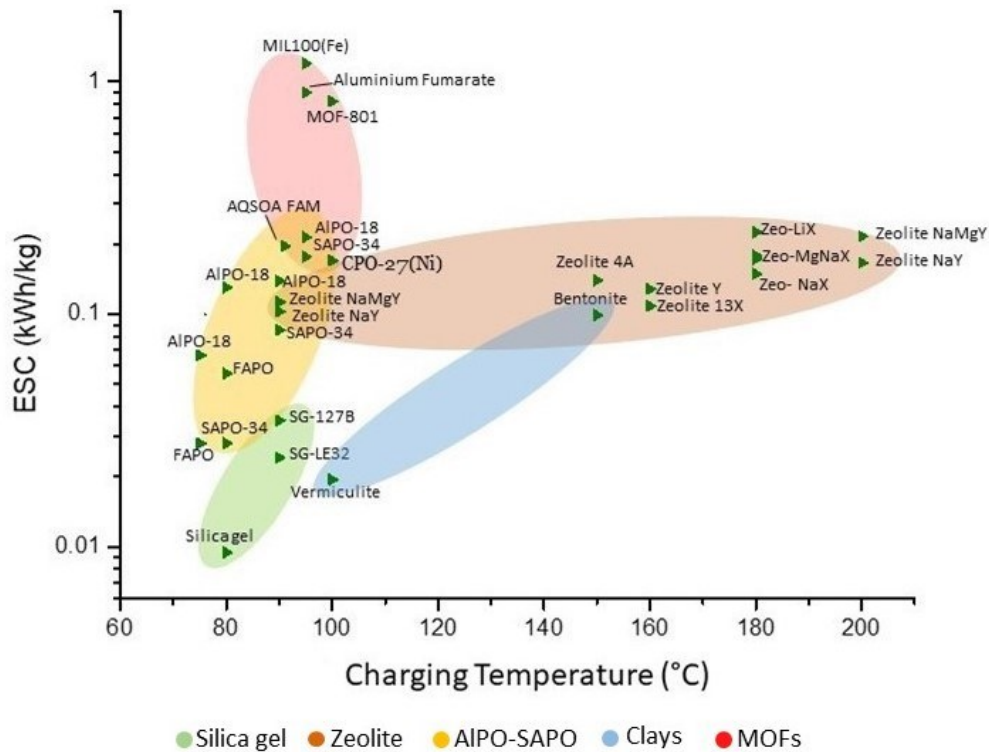
Figure 20: ESC of the main solid sorption materials with regard to the charging temperature

Table 3: Performances of the main solid sorbent materials for STES systems. Where available, we also reported the specific cost of the stored energy

Material	Tc [°C]	Td [°C]	Additional information	Water uptake [g/g]	Method of analysis	ESD [MJ/m³]	ESC [kJ/kg]	SCC [€/kWh]	Ref.
50/50 AA_Z13	120		RH=50%		Open system	137			[97]
70/30 AA_Z13	120		RH=50%		Open system	178			[97]
Activated Alumina	120		RH=50%		Open system	138			[97]
AA + Alkaline	120		RH=50%		Open system	203			[97]

AlPO-18	90	35	T_{cond}=30 °C, T_{ev}= 10 °C		Isosteric		500	719		[83]
AlPO-18	75	35	T_{cond}=30 °C, T_{ev}= 10 °C		Isosteric		240	1499		[83]
AlPO-18	80	35	T_{cond}=15 °C, T_{ev}= 5 °C		Isosteric		470	765		[83]
FAPO 34	80	35	T_{cond}=30 °C, T_{ev}= 10 °C		Isosteric		200	1799		[83]
FAPO 34	75	35	T_{cond}=30 °C, T_{ev}= 10 °C		Isosteric		100	3597		[83]
FAPO 34	90	35	T_{cond}=30 °C, T_{ev}= 10 °C		Isosteric		420	856		[83]
SAPO34	80	35	T_{cond}=30 °C, T_{ev}= 10 °C		Isosteric		100	3597		[83]
SAPO34	90	35	T_{cond}=30 °C, T_{ev}= 10 °C		Isosteric		370	972		[83]
AlPO-18	95	40	P_{ads}=1.2 kPa, P_{des}=5.6 kPa		Calorimetric		770	467		[84]
SAPO-34	95	40	P_{ads}=1.2 kPa, P_{des}=5.6 kPa		Calorimetric		637	565		[84]
AlPO 18	90	35	P_{ads}=1.2 kPa, P_{des}=5.6 kPa	0.305	Calorimetric	970				[40]
SAPO-18	95	40	P_{ads}=1.2 kPa, P_{des}=5.6 kPa	0.254	Calorimetric	1100				[40]
FAPO 34	90	35			Calorimetric	852				[40]
AQSOA FAM Z02	75	35	T_{cond}=30 °C, T_{ev}= 11 °C		Open system		230	360		[105]
AQSOA FAM Z02	81	30	T_{cond}=15 °C, T_{ev}= 6 °C		Open system		330	510		[105]
AQSOA FAM Z02	91	35	T_{cond}=15 °C, T_{ev}= 10 °C		Open system		459	706		[105]
Bentonite	150	20			Calorimetric	890	356	2		[103]
MIL100(Fe)	80	30	P_{des}=12.5 kPa		Calorimetric	875				[106]
MIL101(Cr)	80	30	P_{des}=12.5 kPa		Calorimetric	309				[106]
MIL-125(Ti)-NH$_2$	80	30	P_{des}=12.5 kPa		Calorimetric	1159				[106]

Material					Method				Ref.
MIL100(Fe)	95	40			Open system		4320	208	[107]
Aluminum fumarate	95	40			Open system		3232	278	[107]
Silica gel (SG-127B)_microporous	90	40	T_{cond}=40 °C, T_{ev}= 15 °C		Calorimetric	90	126	36	[108]
silica gel (SG-LE32)_macroporous	90	40	T_{cond}=40 °C, T_{ev}= 15 °C		Calorimetric	54	87	52	[108]
Silica gel	80	35	T_{cond}=10 °C, T_{ev}= 4 °C		Isosteric	14	34	132	[109]
Vermiculite	100				Calorimetric	9.7	70	8	[110]
Zeolite 13X	130				Open system	446			[66]
Zeolite 4A	180	65		0.18	Open system	450	643	14	[67]
Zeolite 4A	150	65		0.14	Open system	353	504	10	[67]
Zeolite CaNaA-60	180		T_{cond}=27 °C, T_{ev}= 1 °C	0.162	Open system	418	623	7	[65]
Zeolite LiX	180		T_{cond}=27 °C, T_{ev}= 1 °C	0.244	Closed system	576	810	9	[65]
Zeolite MgNaX	180		T_{cond}=27 °C, T_{ev}= 1 °C	0.212	Closed system	396	630		[65]
Zeolite NaX	180		T_{cond}=27 °C, T_{ev}= 1 °C	0.192	Closed system	461	536	8	[65]
Zeolite 13X	80	23		0.175	Open system		590	10	[68]
Zeolite Ce2-13x	80	23		0.15	Open system		700	12	[68]
Zeolite NaMgY	200	40	T_{cond}=10 °C, T_{ev}= 10 °C		Isosteric		778	10	[111]
Zeolite NaMgY	90	40	T_{cond}=10 °C, T_{ev}= 10 °C	0.418	Isosteric		307		[111]
Zeolite NaY	90	40	T_{cond}=10 °C, T_{ev}= 10 °C	0.335	Isosteric		406	13	[111]
Zeolite NaY	200	40	T_{cond}=10 °C, T_{ev}= 10 °C		Isosteric		599	34	[111]
Zeolite Y	160	40	T_{cond}=40 °C, T_{ev}= 5 °C		Calorimetric	205	461	26	[112]
MOF-801	100	30			Isosteric method		2960	17	[113]

							[114]
CPO-27(Ni)	100					612	8
MIL125-NH$_2$	90	30	T_{cond}=30 °C, T_{ev}= 10 °C	0.42	Calorimetric	1100	[115]

Table 4: Commercial price of the main solid sorbent materials for STES systems

Material	Price [€/kg]	Material	Price [€/kg]
Zeolite 4	1.2	Silica gel	1.2
Zeolite 13X	1.6	Expanded clay	0.2
Zeolite Y	1.1	Pumice	0.15
Zeolite NaX/LiX	1.8	AlPO	100
Zeolite NaY	2.9	SAPO	100
Bentonite	0.17	FAPO	100
Vermiculite	0.16	MWCNT	4.0
Activated Alumina	0.94	MOF	250

Table 5: Physical properties for popular sorbent materials used in STES

Material	Bulk density [g/cm^3]	Pore volume [cm^3/g]	Pore Diameter [nm]	Surface area [m^2/g]	Specific heat [J/(gK)]	Thermal conductivity [W/mK]	Ref.
Silica gel (siogel®)	0.62-0.8	0.40	2.0	800	0.6-0.8	0.112	[116]
Activated Alumina	0.66	0.51		469		12-38.5	[117]
AlPO-18		0.53		589			
FAPO 34		0.15		423		9.4	[118]
SAPO34		0.25		710			
SAPO-18		0.23		597			[119]
AQSOA FAM Z02	0,24	0.38		650-770		0.204	[120,121]

Bentonite		0.13		64	0.301-1.337	[122]
MIL100(Fe)		0.82		1549		[92]
MIL101(Cr)		2.1		4549		[92]
MIL-125(Ti)-NH$_2$		0.47	0.6-1.1	1160		[92]
Aluminum fumarate		0.25	1.7	1156	0.102	[123]
Vermiculite	0.16-0.19	0.0064		1.4	0.058-0.071	[124]
Zeolite 13X		0.14	7.28	310	0.08-0.13	[125]
Zeolite 4A		0.25	58.14	559	0.15	[125,126]
Zeolite NaX		0.16	10	570	0.4	[127,128]
Zeolite NaY			9.42	626	0.0065–0.25	[129,130]
Pumice		10.9		0.5	0.433-0.177	[131]
MOF-801		0.55	0.74	899	0.025-0.03	[132,133]

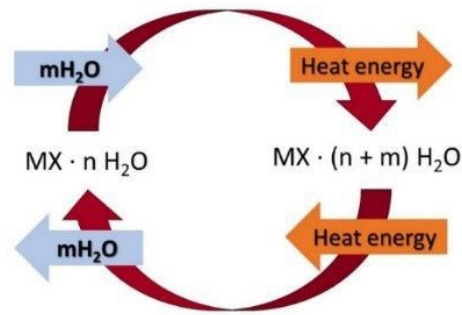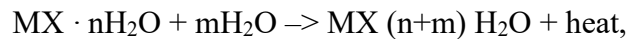## 3.3 Hydrated salts for thermal energy storage

Figure 21: Schematic of the reaction of salt hydration and dehydration

Chemical reactions for TES applications primarily involve hydration/dehydration reactions of salt hydrates according to the following overall reaction:

$$MX \cdot nH_2O + mH_2O \rightarrow MX (n+m) H_2O + heat,$$

where MX represents the anhydrous salt (see **Figure 21**). Hence, hydration is an exothermic reaction with a corresponding heat release. Donkers *et al.* [134] recently performed a literature review to collect and analyze the thermodynamic data of a large number of salt hydrate reactions (563 reactions); they also evaluated the theoretical possibilities and limitations of salt hydrates as thermochemical materials for seasonal energy storage. The working conditions of the system were determined using a phase diagram of the thermochemical material. The phase diagram P(T) indicates the conditions under which hydration–dehydration occurs. Examples of P(T) during charging and discharging in a closed system are represented in **Figure 22**. During discharging, the initial material in the TCM reactor is $MXmH_2O$, and the temperature is T_{w1}, which means that the vapor pressure is $P(T_2)$. The applied conditions around the material are above the equilibrium line between $MX \cdot mH_2O$ and $MX \cdot nH_2O$; therefore, $MXnH_2O$ spontaneously hydrates into $MX \cdot mH_2O$. Consequently, the temperature of the system increases because the reaction is exothermic (**Figure 22**, point 2→3). At temperatures near T_h, both phases, $MX \cdot mH_2O$ and $MX \cdot nH_2O$, can exist. Because the vapor pressure must remain constant, the temperature of the water vessel in the system must be kept constant, that is, the evaporation heat of water must be overcompensated by heating water via heat exchangers (**Figure 22**, point 3). During charging (desorption), the material is heated to a particular temperature T_d with a heat exchanger, and the vapor pressure applied to the system is at P_d (**Figure 22**, point 6). If the vapor pressure is higher than that of the water vessel, the material dehydrates. Because the dehydration reaction is endothermic, the temperature decreases until T_{w2} (**Figure** 22, point 6 → 7). The vapor condenses in the water vessel, releasing the heat of condensation.
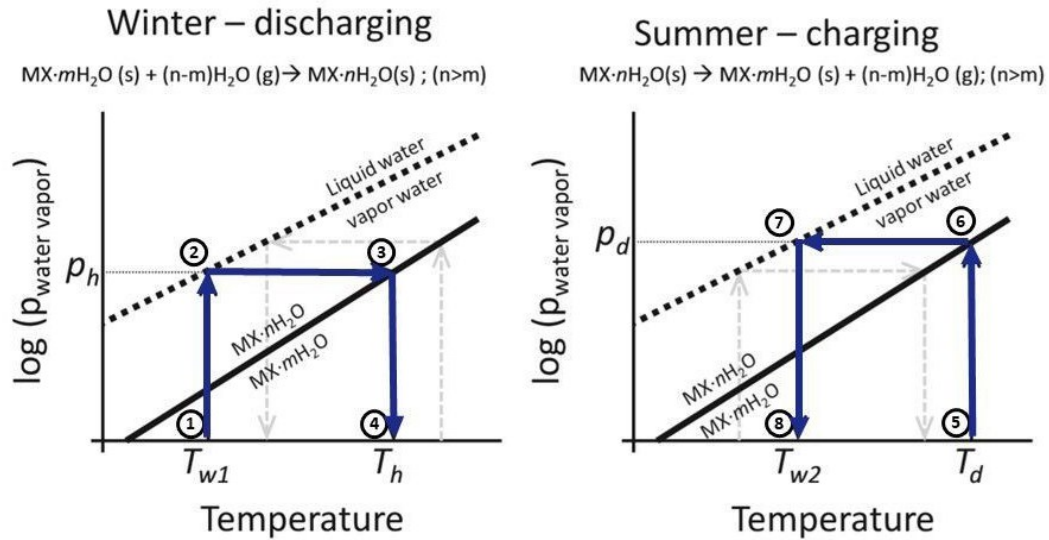
Figure 22: Curve of log(P) with respect to temperature, which represents a common cycle of charging (right) and discharging (left) for a typical sorption thermal energy storage system with hydrated salts [134].

Several aspects must be considered when selecting appropriate thermochemical materials. ESD and ESC may be as high as possible. However, the heat-storage system performance only partially depends on the material storage capacity because the choice of the system (open or closed) influences the effective storage performance.

In addition to hydration and dehydration temperatures, which are key parameters for all sorbent materials, the volume variation during hydration, melting temperature, price, safety, and chemical stability are also important [134].

In addition to hydrated salts, NH_3-salt couples are sometimes used as thermochemical storage materials [40]. As shown in Table 6, they exhibit high energy storage densities. However, they can only be used in closed systems because sorbates and sorbents are not separated from the environment in open systems.

Closed systems require additional volume for the condenser-evaporator and sorbent-fluid storage; hence, they do not always meet the reduced-space demand. However, higher additional costs due to the system, apart from the active material, are required for closed systems, than those for open systems. Hence, a comprehensive comparison between water-hydrated salts and NH_3-salt can be done in the case of closed system. Examples of the main solid materials used in STES are reported in Table 6.

Table 6: Performances of chemical sorbent materials for STES systems

Material	Price [€/ton]	Tc [°C]	Td [°C]	Additional information	ESD [MJ/m³]	ESC [kJ/kg]	SCC [€/kWh]	Ref.
BaCl$_2$*H$_2$O/BaCl$_2$	680	80			880	230	11	[134]
CaCl$_2$*2H$_2$O/CaCl$_2$	160	95	95		1100	510	1	[134]
Li$_2$SO$_4$*H$_2$O/LiSO$_4$		103			900	410		[134]
MgCl$_2$*6H$_2$O/MgCl$_2$*2H$_2$O	154	118	50		1270	550	1	[134]

MgSO$_4$*6H$_2$O/MgSO$_4$*H$_2$O	77	72		2370	890	0.3	[134]
MgSO$_4$*7H$_2$O/MgSO$_4$	77	122		2800	1050	0.3	[134]
Na$_2$S*5H$_2$O/Na$_2$S+0.5H$_2$O	348	80		2700	2910	0.4	[134]
SrBr$_2$/6H$_2$O	2400	90		1904	800	11	[135]
LiCl/H$_2$O		72		2080	1000		[136]
BaCl$_2$/NH$_3$	680	56	P$_{ads}$=1.167	2833	1470	2	[137]
CaCl$_2$/NH$_3$	160	99	P$_{ads}$=1.167	2423	2240	0.3	[137]
FeCl$_2$/NH$_3$	845	186	P$_{ads}$=1.167	2560	1620	2	[137]
MnCl$_2$/NH$_3$	1936	152	P$_{ads}$=1.167	2246	1510	5	[137]
NaBr/NH$_3$	2011	51	P$_{ads}$=1.167	2887	1800	4	[137]
NH$_4$Cl/NH$_3$	231	48	P$_{ads}$=1.167	1264	1650	0.5	[137]
NiCl$_2$/NH$_3$	3500	259	P$_{ads}$=1.167	1757	1830	7	[137]
SrCl$_2$/NH$_3$	920	96	P$_{ads}$=1.167	2794	1830	2	[137]

Salts based on metal halides are the most widely used for reactions with ammonia. The large number of halides and the different phases of coordination reactions are able to cover a wide temperature range from -50 to 350 °C [138,139]. Ammonia has a lower latent heat of vaporization than water and a boiling point at -34 °C at ambient pressure; therefore, compared to water, it has a wider range of operating conditions and can be operated at higher pressure thus contributing to better heat and mass transfer[140]. Energy storage for the salt-NH$_3$ pair can only be used in a closed system[141], with a similar configuration and processes to those explained previously in Chapter 2.1. Performance based on salt-ammonia reactions is strongly influenced by the efficiency of heat and mass transfer in a fixed-bed reactor. Pecked beds of granular metal salts have low thermal conductivity because of the inherent low thermal conductivity of metal halides and poor particle-to-particle contacts[142]. In addition, ammonia diffusion within the reaction bed may be hindered by pore clogging due to volumetric expansion or salt swelling during the adsorption reaction between ammonia and salt[40]. These two factors may prolong the reaction time thus reducing the thermal power density. Therefore, the use of composites, which consist of a pure salt impregnated in a porous host matrix can improve heat and mass transfer and consequently the dynamic performance of adsorption cycles [143–145]. However, such strategy can reduce the specific adsorption capacity of the salt and consequently the energy density[26]. This is because they contain a less effective reactive adsorbent per unit of mass or per unit of volume. In addition, the mass density of the composite and the mass ratio between the metal salt and the matrix must be selected rationally to balance the heat and mass transfer performance. Moreover, another challenging aspect that can lead to a certain degree of discrepancy between the performance achieved in practice and the ideal theoretical results is that metal halide-ammonia working pairs commonly exhibit a hysteretic phenomenon. This implies the irreversible loss of energy during a complete adsorption-desorption cycle [143,146]. In ammonia-based chemisorption, kinetics is a very important knowledge to define the size, the optimal design and to control the system. Currently, information on chemisorption kinetics is relatively scarce [147]. Different kinetic models have been proposed by various authors[148,149], who have studied disparate reactive media contained in different reactors having different geometrical structure at various scales, and meanwhile

have adopted several assumptions to simplify their modeling to a greater or lesser extent for their specific purposes and objectives. The transient nature of chemisorption is related to the kinetics of the solid-gas reaction and the properties of the reactor/reactant with regard to heat and mass transfer, which may have an impact on the determination of kinetic parameters in numerical solving a set of differential equations. Bao et al. [150] reviewed and discussed several kinetic models of salt and ammonia chemisorption and summarized and listed the kinetic parameters in the different models.

3.4 Composite sorbent materials

Physically porous sorbents offer a stable performance, but low energy density and energy capacity. Chemical sorbents are characterized by higher storage capacities, although the phenomenon of deliquescence, which may affect grain stability, limits their performance. Recently, several studies proposed a family of new working materials for solid sorption, consisting of "hygroscopic salts inside a porous matrix with open pores" [151]. In this case, the porous structure of the host matrix provides numerous gas diffusion paths; hence, the material has sufficient vapor permeability to promote salt hydration. In addition, the agglomeration of salts is hindered because it is enclosed in a solid matrix. As previously shown, the salt adsorption ability of the fluid phase depends on the chemical nature of the salt. However, several studies have shown that the performance of the composite sorbent–sorbate pair is not the result of a simple addition of the sorption of the bulk salt and host material [152,153]. It was observed that the salt sorption ability increased, owing to confinement in a microporous matrix, which also hindered the hysteresis behavior of the adsorption-desorption cycles. Hence, space confinement causes changes in the thermodynamics of salt solutions. However, no final explanation has been identified in the current literature [154]. Moreover, the behavior of a porous host and salt when combined strictly depends on the nature of both the components and external working conditions. Thus, further research on this phenomenon is necessary. In **Figure 23**, the charging/discharging mechanism of the material is schematically represented, and the main steps are described.
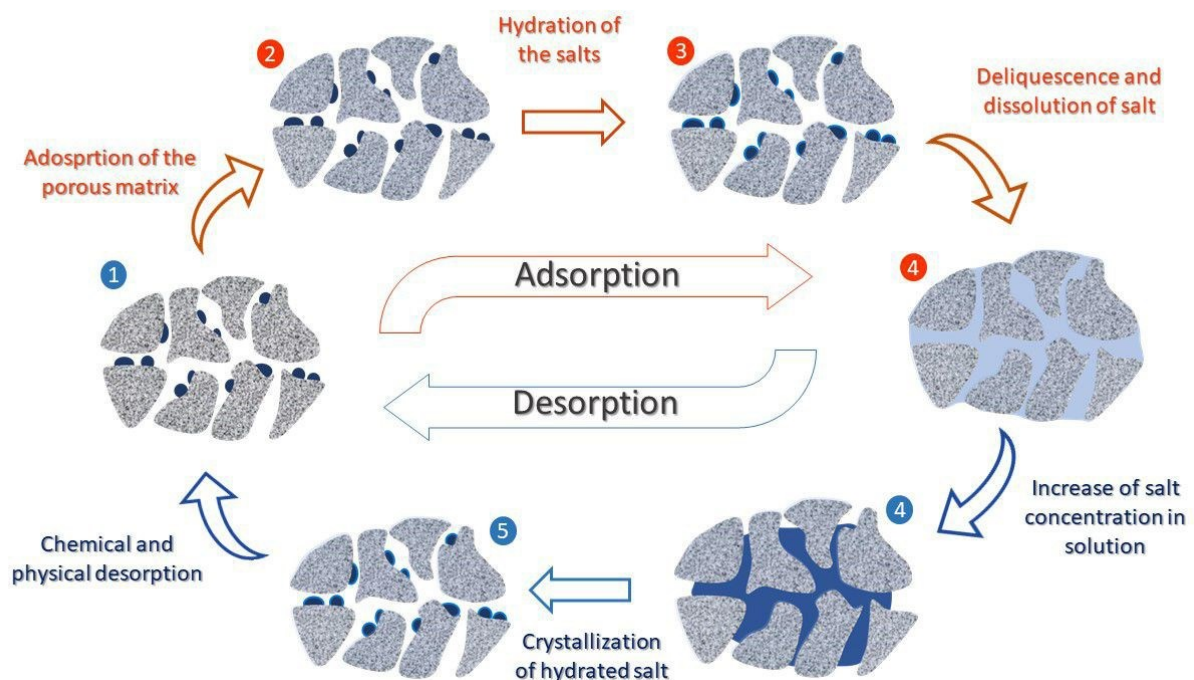

Figure 23: Schematic of the mechanism of adsorption and desorption for a "hygroscopic salt in porous host" material.

During the energy discharge phase (adsorption):

1→2: the porous matrix adsorbs water (generally due to van der Waals forces);

2→3: the anhydrous salt undergoes chemical sorption, and salt hydrates are formed;

3→4: deliquescence and dissolution of salt occurs into pores, adsorption of vapor continues, and the salt concentration in solution decreases.

During the energy charge phase (desorption):

4→5: the dilute solution increases in concentration;

5→6: crystallization of the saturated salt solution and efflorescence of crystals occur;

6→1: chemical desorption and physical desorption take place, in sequence.

The same mechanism is presented in **Figure 24**, where the sorbate pressure is reported with respect to temperature.
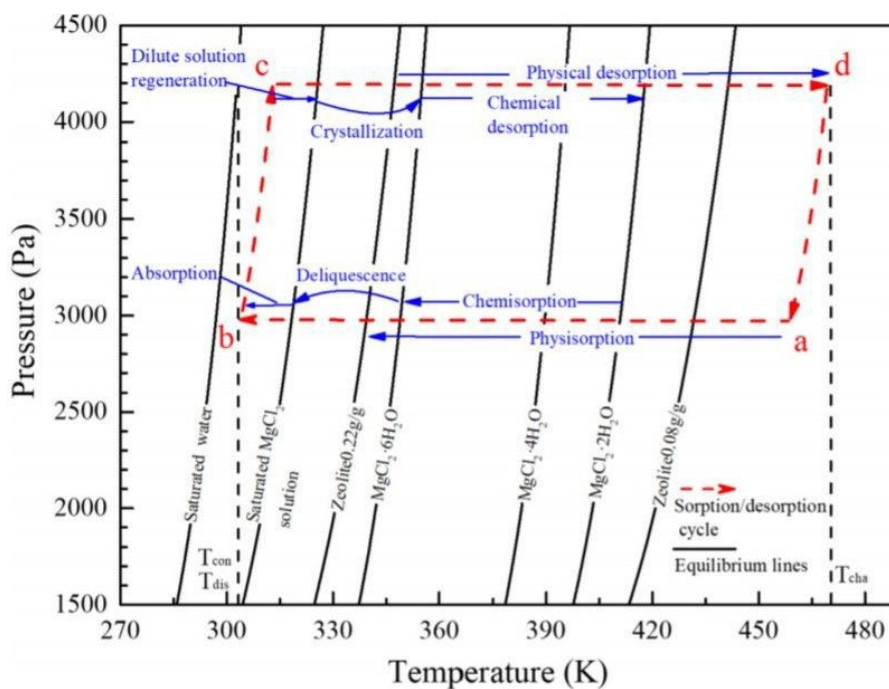

Figure 24: P(T) plot of thermochemical energy storage cycle using $MgCl_2$-zeolite composite sorbent [155]

A higher sorption capacity is reached when deliquescence occurs, and the volume of the final solution is equal to the volume of the pores. It is generally observed that the sorption ability of the system increases with an increase in the amount of salt (which provides the most relevant contribution to heat release). However, an excessively high salt content may result in the oversaturation of the matrix during the hydration step. During adsorption, the volume of the aqueous salt solution exceeds the available pore space and leaks out of the matrix.

However, large amounts of salt can hinder the sorption dynamics, owing to the so-called "blocking effect." Grekova *et al*. [156] reported a 30% reduction in the pore volume when passing from vermiculite to a vermiculite-LiCl composite. Elsayed *et al.* [157] showed how the water sorption curve of MIL-101/$CaCl_2$ changes owing to the partial filling of pores by salt. In general, the sorbate phase occupies almost the entire pore space of the matrix; hence, the mass-transfer barrier strengthens [158]. Therefore, evaluation of the amount of salt is necessary when introducing it into the porous host [159].

The most common method for synthesizing a composite is the impregnation of a matrix with an aqueous solution [152]. First, the porous matrix is dried to remove all water adsorbed on its free surface. The material is then impregnated with a solution of the salt responsible for the sorption process. At this stage, two different methods can be applied: dry impregnation or wet impregnation. The first (dry, also called incipient wetness impregnation) involves volume of solution V_s, which is equal to pore volume of the matrix V_p. While the liquid soaks quite quickly into the porous matrix, salt ions may take more time; hence, the sample may remain in the wetting state for several hours[160]. In the second case (wet), V_s is higher than V_p. Hence, the matrix is dipped in the solution for several hours, after which the excess solution is removed using a vacuum desiccator [152]. In all cases, the quantity of salt dispersed in the matrix and its distribution depend on three factors: the concentration of the salt solution, the possible chemical interactions between the salt and matrix, and the drying scenario.

In the case of wet impregnation, the salt can partially precipitate on the outer parts of the grains during drying, thereby forming large crystals. Hence, additional treatments during the synthesis of the composite must be considered to dissolve and remove these crystals. This has not been observed for dry impregnation [153], which is also preferred owing to the lower volume of solution that is required.

An additional and more recent approach is referred to as the "*in situ*" method. It involves the introduction of the selected salt directly during the synthesis of the host material. This is the case for silica gel, which is typically obtained from organic precursors. A particular percentage of the salt hydrate is slowly added to the siloxane matrix under vigorous mixing until a homogeneous slurry is obtained. Finally, the foaming reaction must be performed in an oven at a controlled temperature [161]. A preliminary study demonstrated that this method can also be conducted using a nonconventional matrix, such as cement. The cement is prepared by mixing water and cement powder and curing it for several days to achieve a complete hydration reaction. Instead of water, a saturated solution of the salt can be used [162].

During discharging (adsorption), sorbate uptake, which is usually expressed as m/m_0, can also be described as the number of sorbate molecules per molecule of salt. Low values of thermal conductivity can significantly limit the heat-transfer rate in an STES, thereby reducing the overall system performance. It is well known that the higher the porosity, the lower the thermal conduction of the material. However, inorganic salts are known to be good thermal insulators. Therefore, heat transfer enhancement techniques are often used to overcome the low thermal conductivity of STES systems, for example, fins and metallic meshes. However, the latter increases the total cost of the devices, owing to the use of extra parts and a more complex design. This decreases the effective TES density, owing to the extra volume. Hence, optimization of the thermal conductivity without affecting the thermal energy performance is still being researched. Lele *et al.* [163] reported that the effective thermal conductivity of a salt can be increased by approximately two or three times when impregnating porous matrices with salt. This may be due to the reduction in the air volume inside the material, which creates a better heat path. Another solution, which has been recently explored in the literature, involves the introduction of highly conductive elements inside the adsorbent, which increases the overall thermal conductivity. Shere *et al.* [164] added multi-wall carbon nanotubes (1% wt) to a zeolite 13x–$MgCl_2$ composite, which improved the conductivity by 35%. Elsayed *et al.* [157] reported an enhancement in the thermal conductivity of MIL-101(Cr) by more than 2.5 times when using hydrophilic graphene oxide, both physically mixed or directly incorporated during the synthesis of MIL-101(Cr). Finally, expanded graphite has recently been investigated as a porous and highly thermally conductive host for salt hydrates. The choice of carbonaceous materials as porous matrices does not enable very high values of ESC and ESD, but drastically increases the heat transfer; thus,

finned heat exchangers may not be necessary. In some cases, the incompatibility between the structures of graphite and the hydrate salt can cause the formation of large salt aggregates, which affects the water adsorption performance. Salviati *et al.* [165] recently proposed the production of graphite composites encompassing a polyelectrolyte binder (polyallyldimethylammonium chloride, PDAC), to enhance the compatibility between the salt and matrix. A selection of the most commonly used composite materials for STES is reported in **Figure 25** (ESC vs. charging temperature); additional information is given in Table 7.
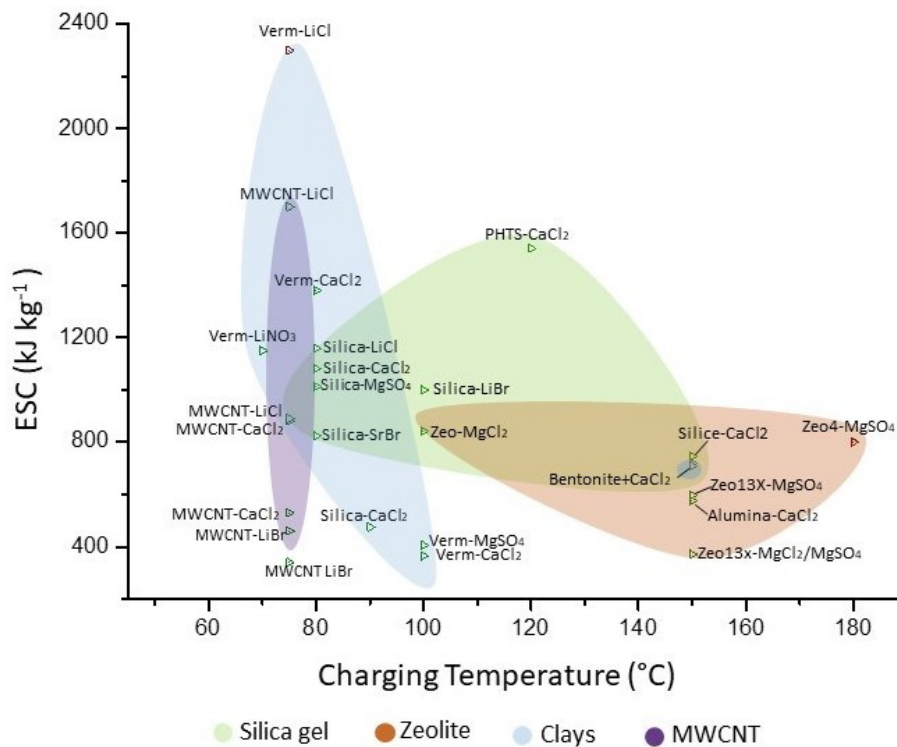

Figure 25: ESC of the main composite sorption materials

Table 7: Performances of composite sorbent materials for STES systems

Sorption material	Price [€/ton]	T_c [°C]	T_d [°C]	Additional information	Water uptake [g/g]	Method	ESD [MJ/m³]	ESC [KJ/Kg]	SCC [€/kWh]	Ref.
Alumina + CaCl₂ (14.4%)	828	150	20			Calorimetric method		576	5.2	[103]
Bentonite + CaCl₂ (15%)	165	150	20		0.2	Calorimetric method		719	0.6	[103]
Bentonite + CaCl₂ (40%)	123	150				Open system	490	705	0.8	[67]
EG + CaCl₂ (87%)	163	120				Calorimetric method	600	2000		[166]
EG + CaCl₂ (87%)		100				Calorimetric method		1451		[167]
EG + SrBr₂ (80%)		80				Calorimetric method		500		[168]
EG + SrBr₂ (80%)		150				Calorimetric method		600		[168]
Expanded clay + SrBr₂ (40%)		110	20				313	711	5	[169]

Material						Method				Ref
MIL-100 (Fe) + CaCl$_2$ (46%)	1080	80	30		0.57	Calorimetric method	749	1206		[106]
MIL-101 (Cr) + CaCl$_2$ (62%)	290	80	30		0.75	Calorimetric method	1116	1746		[106]
MWCNT CaCl$_2$ (53%)	251,2	75	15	Tcond=15 °C, Tev= 5 °C	0.18	Isosteric method	477	530	2	[170]
MWCNT CaCl$_2$ (53%)	272,8	75	15	Tcond=30 °C, Tev= 10 °C	0.31	Isosteric method	792	880	1	[170]
MWCNT LiCl (44%)	272,8	75	35	Tcond=15 °C, Tev= 5 °C	0.57	Isosteric method	2380	1700	3	[170]
MWCNT LiCl (44%)	1412	75	35	Tcond=30 °C, Tev= 10 °C	0.3	Isosteric method	1246	890	6	[170]
MWCNT+LiBr (42%)	1412	75	35	Tcond=15 °C, Tev= 5 °C	0.31	Isosteric method	782	460	20	[170]
MWCNT+LiBr (42%)	2542	75	35	Tcond=30 °C, Tev= 10 °C	0.23	Isosteric method	578	340	27	[170]
PHTS + CaCl$_2$ (10%)	2542	120	40	Tcond=10 °C, Pdes=12.3 kPa	0.142	Isosteric method	428	1541	3	[171]
Silica gel + LiBr (29%)	1141	100	40	Pads=11.4 kPa, Pdes=11.4 kPa	0.8	Isosteric method		1000	9	[152]
Silica gel + LiCl (10%)	2457	80	35	Tcond=10 °C, Tev= 4 °C		Isosteric method	176			[109]
Silica gel + LiCl (31%)	1395	100	40	Pads=11.4 kPa, Pdes=11.4 kPa	0.8	Isosteric method		1000	6	[152]
Silica gel + LiCl (40%)	1700	80	35	Tcond=10 °C, Tev= 4 °C		Isosteric method	854	1159	6	[109]
Silica gel + SrBr (58%)	1830	80	30			Calorimetric method	730	825	8	[172]
Silica gel CaCl$_2$ (43%)	1917	80	30	Tcond=10 °C, Pdes=12.5 kPa	0.77	Calorimetric method	760	1081	3	[173]
Silica gel + CaCl$_2$ (14%)	781,3	150	20			Calorimetric method		746	5	[103]
SiO$_2$ + MgSO$_4$ (58%)	1097	80				Calorimetric method	480	1012	2	[174]
Vermiculite + LiCl (59%)	570	75	35			Open system	910	2300	2	[175]
Vermiculite + LINO$_3$ (59%)	1660	70	28	Tcond=35 °C, Tev= 10 °C		Calorimetric method	450	1150	18	[176]
Vermiculite CaCl$_2$ (86%)	5877	120				Calorimetric method	1200	2000	0.3	[166]
Vermiculite SrBr (63%)	160	100				Calorimetric method	379	1656	3	[158]
Vermiculite+CaCl$_2$	1571	80	25	Pdes=12 kPa		Calorimetric method	760	1380	0.4	[177]
Zeolite 13X + MgCl$_2$/MgSO$_4$ (7,5/7,5%)	160	150	30			Calorimetric method		370	13	[164]
Zeolite 13X + MgSO$_4$ (15%)	1343	150	25			Calorimetric method	648	597	8	[178]
Zeolite 4A + MgSO$_4$ (10%)	1338	180			0.23	Open system	640	800	5	[67]
ZeoliteNaX + MgCl$_2$ (12.6%)	1106	100	30			Calorimetric method		842	7	[179]

4. Comparison between sorbent materials

A comparison among the different sorbent material categories is reported in this section in terms of both energy and economic KPIs. In particular, **Figures 26** and **27** show the ESD and ESC for different charging temperatures, respectively.
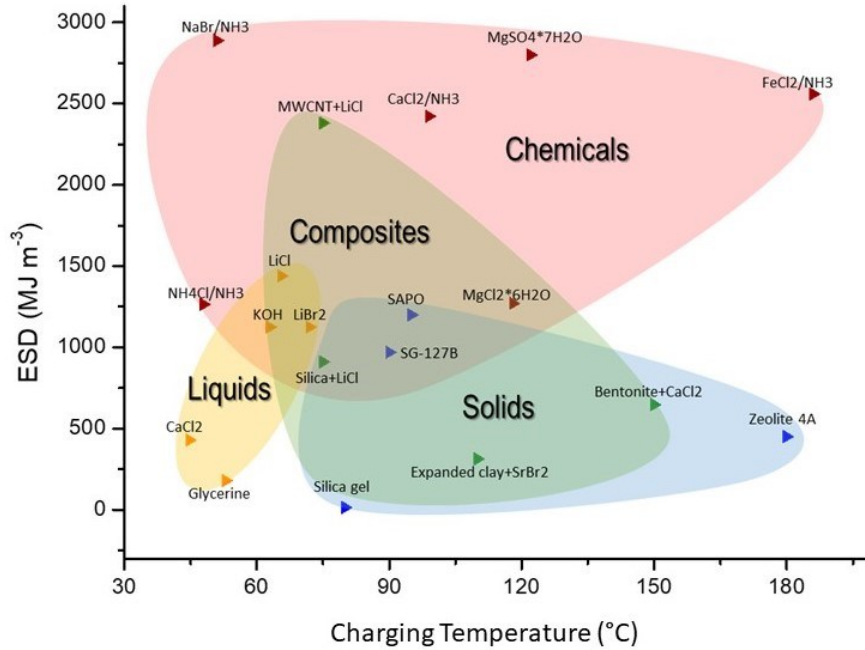

Figure 26: ESD of the different sorption material categories with regard to the charging temperature (the colored domains represents materials reported in table 2,3,6,7).
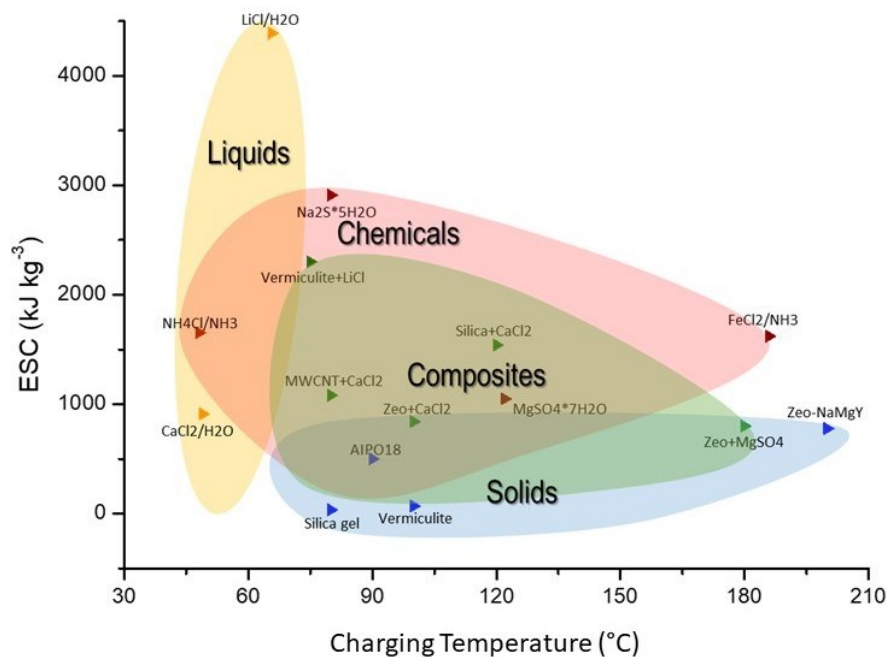

Figure 27: ESC of the different sorption material categories with regard to the charging temperature.

When selecting the most suitable sorption material, the charging temperature should be in a suitable value range. As an example, if thermal solar by standard collectors is the energy source, the charging temperature is expected to be sufficiently low in order to maximize exploitation of the renewable

energy source. At the same time, to minimize the material volume (or weight) required for a given application ESD (or ESC) shall be maximized. Because the relationship between ESC and ESD depends on the bulk density of the material (or bed density), high values of ESC do not necessarily correspond to high values of ESD. The plotted contour for each class of materials considers all the data reported in the previous tables. For clarity, only a few names are reported in the charts.

Figure 27 shows that sorbent for chemisorption appear to be the most performant materials in terms of ESD (720–2900 MJ/m^3), ranging from low to high charging temperatures (80–190 °C). NaBr/NH$_3$ has the best combination of high-energy performance and a low charging temperature. However, it can only be used in closed systems because in open systems, the sorbate and sorbent are not separated from the environment; hence, NH$_3$ cannot be involved in the sorption mechanism. However, MgSO$_4$·7H$_2$O presents high values of ESD and is able to release 2800 MJ m^{-3} at a charging temperature of approximately 120 °C. It appears suitable for both closed and open systems with water as the sorbate. Nonetheless, such materials are plagued by the problem of deliquescence, which affects the grain stability and may limit the performance of materials as sorbents after a few cycles. In contrast, solids (blue shadow) present lower values of ESD (10–1200 MJ/m^3), and some of them require charging temperatures higher than 150 °C. The latter condition, i.e., overcoming 150 °C, is not always accessible using solar collectors; hence, not all solid sorbents appear suitable materials for STES in low-temperature solar applications. Moreover, the performance of the entire class worsens in terms of the ESC. While a wide range of ESD values is covered, from 14 MJ/m^3 for silica gel to 1200 MJ/m^3 for SAPO-34, only a range of less than 800 kJ/kg, from 70 kJ/kg for vermiculite to 810 kJ/kg for zeolite 4X, is observed for ESC. Composites (green shadow) represent a good compromise between the two categories, with reasonable energy storage performance when the charging temperature remains below 150 °C. Finally, liquids can operate at lower temperatures than other categories of sorbents. This condition is advantageous in terms of the heat required for charging. However, despite liquids reaching appreciable ESC values of 4400 kJ kg^{-3}, the low density of such materials causes the entire category to offer only relatively low ESD values, without exceeding 1450 MJ/m^3. Moreover, some liquids, including KOH, NaOH, and ammonia, are harmful, especially to human tissues. Finally, all the salt-based solutions present a degree of corrosion against stainless steel. The latter condition causes a reduction in the sorbate tank lifetime, thereby leading to additional costs for its maintenance or replacement [180].

Finally, a comparison between adsorbent categories in terms of storage capacity cost (SCC) is of interest. SCC is defined as

$$SCC = \frac{Euro/ton}{ESC \cdot 1000} \cdot 3.6,$$

and it is generally expressed in terms of €/kWh. SCC is the most interesting KPI because it allows for a comparison between materials, considering their commercial price. This is crucial for evaluating the technological feasibility and scalability of a system. Highly performant but expensive materials do not offer a reliable solution for low-temperature TES because their production at the industrial level is not feasible. **Figure 28** graphically reports the €/kWh values (i.e., SCC^{-1}) of the four sorbent classes with respect to the charging temperature, thus displaying the best case toward the top of the graph.
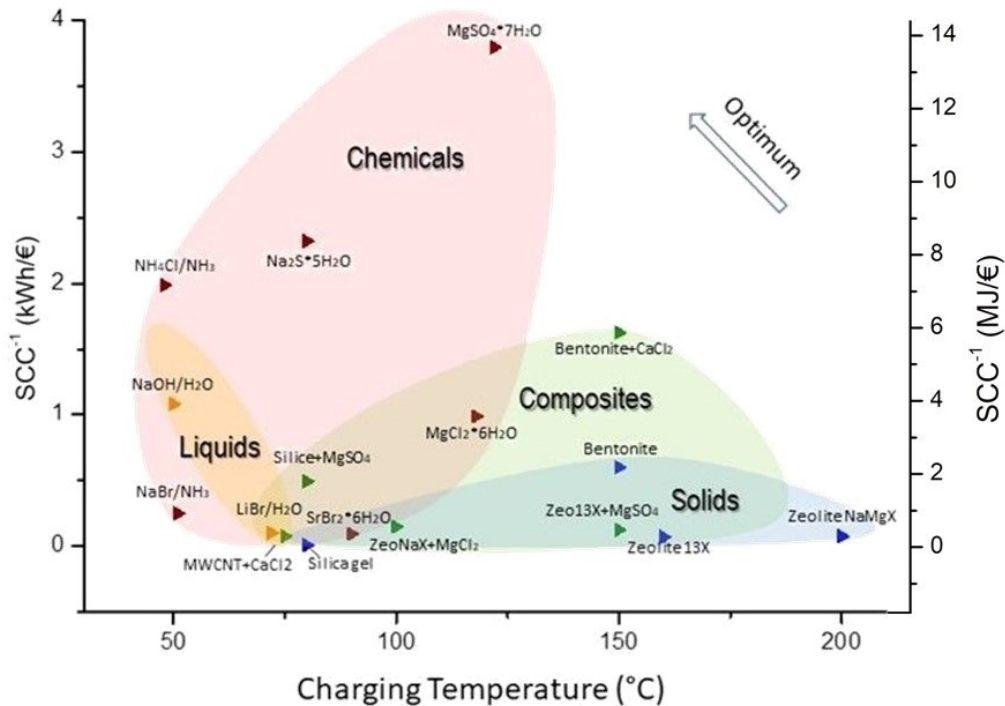
Figure 28: Values kWh/€ for different sorption material categories with regard to the charging temperature.

Upon comparison of **Figures 27** and **28,** liquids partly lose their attractiveness; despite their high ESC, the high material cost causes a sharp decrease in their performance in terms of SCC. However, some chemicals boast a relatively low price; hence, their performance is outstanding. Solid materials invert their trends. The details can be observed by comparing **Figures 20** and **29**. Zeolites have a market price of approximately 2500 €/ton, which is higher than that of bentonite or vermiculite (approximately 160 €/ton). Therefore, zeolites are competitive without consideration of the price. However, zeo-type and metal-oxide-framework materials are commercially available for prices of approximately 100 €/kg and 250 €/kg, respectively, which exceed the price of zeolites and clays by two or three orders of magnitude. Despite their excellent performance when tested in the laboratory, they have not yet provided a suitable and scalable solution for industrial STES systems. Additional studies are still required to determine the most performant materials at affordable prices. Similar considerations can be made for the respective composites by comparing **Figures 25** and **30**.
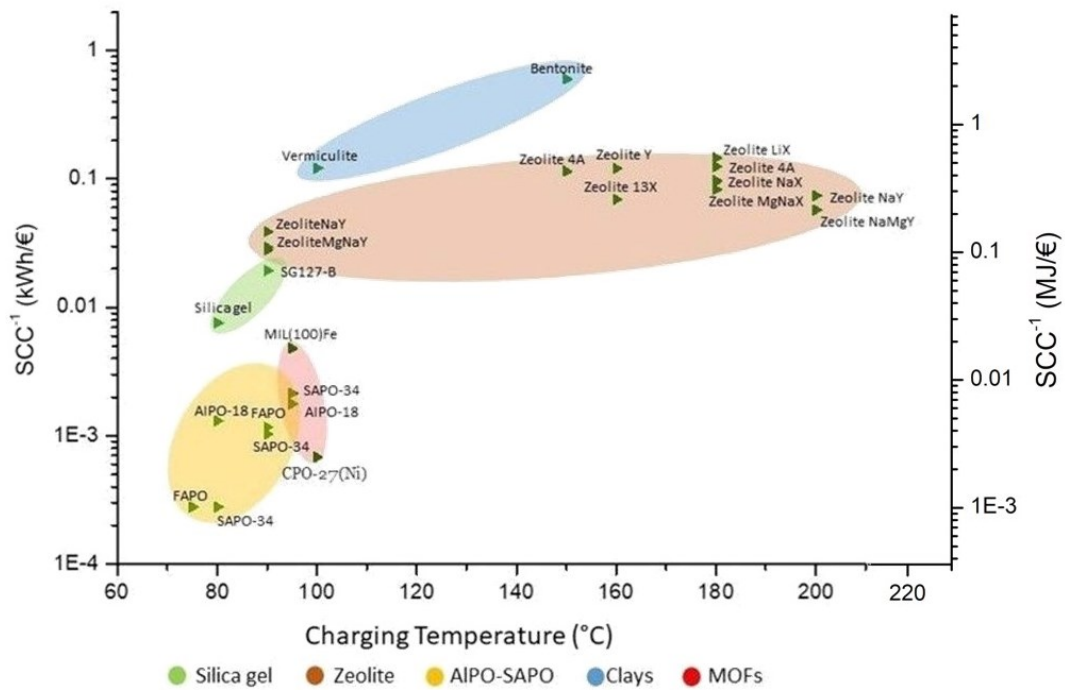
Figure 29: kWh/€ values of different solid sorption materials with regard to the charging temperature.
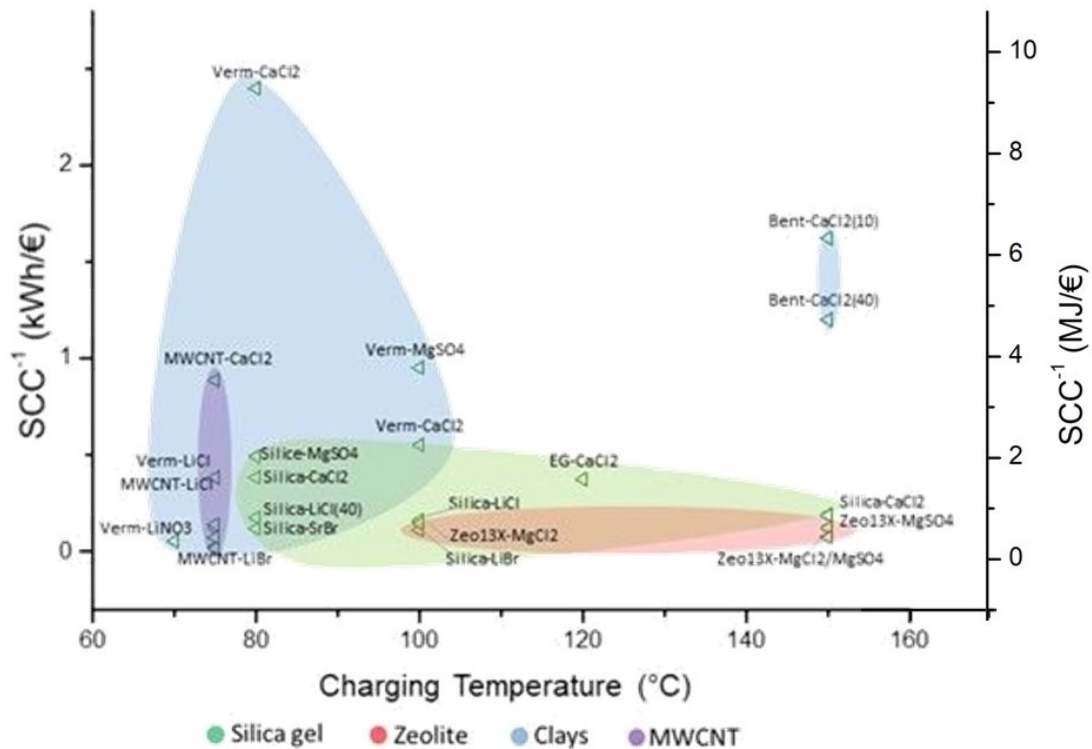

Figure 30: kWh/€ values of different composite sorption materials with regard to the charging temperature.

Finally, a comparison in terms of kWh/€ versus ESD is shown in **Figure 31**. The optimal condition maximizes the storage energy both per unit cost and volume. The latter not only defines the space needed to host the storage system but also contributes in extent to the overall cost of the system, considering the volume of the supporting material (usually AISI316) that structures the reactor. Hence, the cost of the non-active material must be added to the cost of the active material, thus

defining the total cost of the involved material. The kWh/€ versus ESD graph shows that in this case, chemicals occupy the upper right region, which correspond to the optimal conditions of material selection.
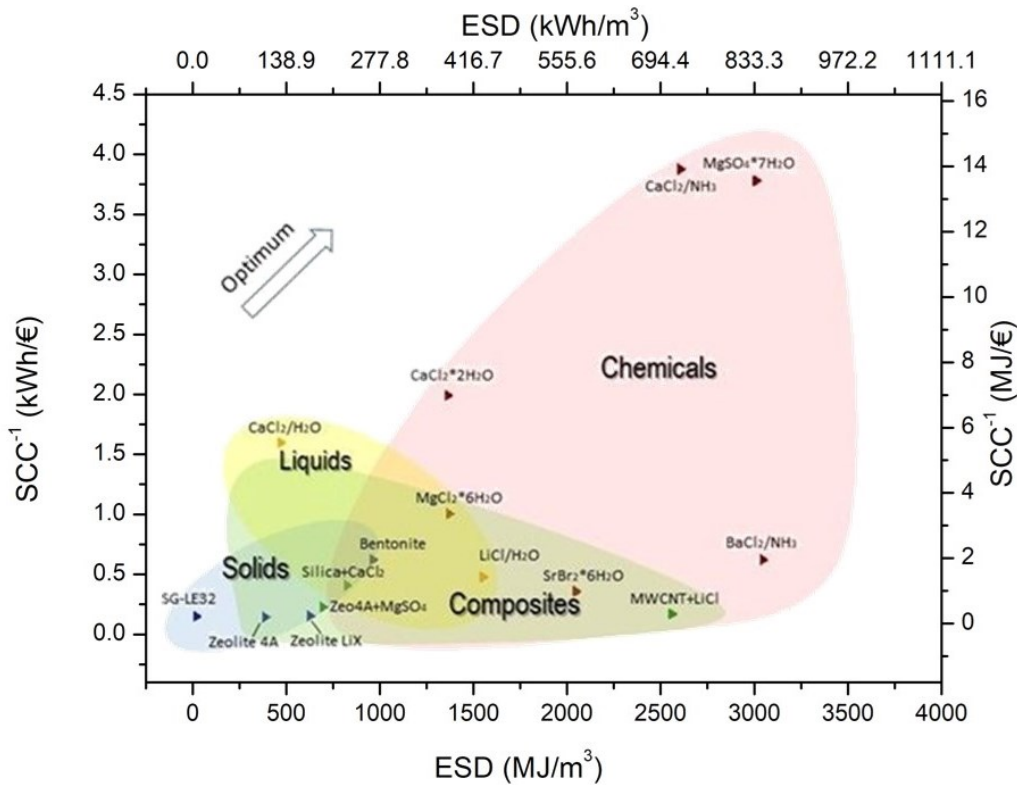

Figure 31: kWh/€ values of different sorption material categories with regard to their ESDs

The different parameters considered (ESD, MJ/m^3; ESC, kJ/kg; SCC, €/kWh; charging temperature) can assist with choosing the best material for a specific situation. Methods and criteria for material selection were studied in detail by Ashby [181]. However, we suggest a procedure to use these graphs suitably. First, an objective must be defined along with the constraints. The objective may be the minimization of mass or volume, or the maximization of stored heat. The constraints may be the temperature limits or a limit on the volume, mass, or cost. By defining constraints, it is possible to exclude areas of the graphs, whereas objectives define the search direction (top left, top right, bottom left, and bottom right). By coupling constraints and objectives, it is possible to determine the best material for a specific application.

5. Conclusion

Among all TES technologies, STES systems exhibit the highest performance in terms of ESC and they may allow the realization of compact seasonal heat storage batteries. Hence, their use can potentially improve the storage capability of renewable thermal energy, thus helping alleviating their intrinsic intermittency nature. However, achieving robust and low-cost sorbent materials still remains a challenge although it is widely recognized to be the key factor for successfully bringing STES to a sufficient technological maturity. A general review of existing sorbent materials (solids, liquids, salts, and composites) was conducted to elucidate the mechanism of TES and its main properties. Several graphs enabled a comparison of single materials and material classes in terms of ESD (MJ/m^3), ESC (kJ/kg), SCC (€/kWh), and charging temperature. Liquids can work at lower charging temperatures than other categories of sorbents. This represents an advantage in terms of the amount of heat (i.e., thermal energy) required for desorption. However, relatively low values of ESD can be achieved

using liquids, not exceeding 1450 MJ/m^3. However, owing to their low density, they offer high ESC values, thus overcoming the limitations associated with the use of other sorbent categories. However, the SCC index shows that liquids are no longer convenient for the chosen application. Despite their high capacity for energy storage, the high cost of raw materials causes the overall performance of liquid-based TES systems to drastically decrease. In addition, security parameters, such as health, flammability, and reactivity, play a crucial role in the exploitation of liquids as sorbents for thermal storage systems. Alternatively, solid sorbents cover a wide range of values in terms of energy performance, from the low storage capacity of silica gel and clays to the higher storage capacity of MOFs, AlPOs, and zeolites. Nonetheless, the latter group of solids is not affordable in terms of price per ton when considering an industrial-scale application. Consequently, for SCC, the performance of all solid sorbents decreases to a low level, owing to their low storage capacity or high material cost. Chemicals appear to be the best sorbent materials in terms of both ESC and ESD. However, it must be noted that sorption couples involving NH$_3$ can only be used for closed systems. Moreover, all chemicals are affected by the problem of deliquescence, which affects the grain stability and severely limits the material performance after a few cycles. Composite sorbents, in which hygroscopic salts are introduced into a porous matrix, thus emerge as a good compromise between the solid and chemical categories with respect to all the energetic performance ratings. The possibility of choosing several porous matrices and chemicals, combining them in different concentrations, and using a variety of methods enables considerable increases in terms of ESC. We hope that this overview on sorbent materials may help in better elucidating the critical roadblocks both in the specific field of sorption based thermal energy storage and hopefully also more in general in sorption based heat transformations (e.g., solar cooling [182]).

Funding sources

References

[1]   E. commission directorate-general for energy, Mapping and analyses of the current and future (2020-2030) heating/cooling fuel deployment (fossil/renewables), 2016.

[2]   D. .E.N.E.R, Communication from the commission to the european parlament, the council, the European economic and social committee and the committee of the regions, 2016.

[3]   I. heat transfer ICAX, Heat Recycling | Seasonal Heat Storage | GSHC | Ground Source Heating and Cooling | Ground Energy | GSHP, n.d.

[4]   A. Ribezzo, G. Falciani, L. Bergamasco, M. Fasano, E. Chiavazzo, An overview on the use of additives and preparation procedure in phase change materials for thermal energy storage with a focus on long term applications, Journal of Energy Storage. 53 (2022) 105140. https://doi.org/10.1016/j.est.2022.105140.

[5]   Y. Zhang, R. Wang, Sorption thermal energy storage: Concept, process, applications and perspectives, Energy Storage Materials. 27 (2020) 352–369. https://doi.org/10.1016/j.ensm.2020.02.024.

[6]   L. Socaciu, Seasonal Sensible Thermal Energy Storage Solutions, Leonardo Electronic Journal of Practices and Technologies. 10 (2011) 49–68.

[7]   Hauer, Thermal Energy Storage,IEA-ETSAP and IRENA Technology-Policy (January 2013), n.d.

[8]   A.F. Regin, S.C. Solanki, J.S. Saini, Heat transfer characteristics of thermal energy storage system using PCM capsules: A review, Renewable and Sustainable Energy Reviews. 12 (2008) 2438–2458. https://doi.org/10.1016/j.rser.2007.06.009.

[9]   Y. Zhang, G. Zhou, K. Lin, Q. Zhang, H. Di, Application of latent heat thermal energy storage in buildings: State-of-the-art and outlook, Building and Environment. 42 (2007) 2197–2209. https://doi.org/10.1016/j.buildenv.2006.07.023.

[10] B. [Eanest Jebasingh, A. [Valan Arasu, A comprehensive review on latent heat and thermal conductivity of nanoparticle dispersed phase change material for low-temperature applications, Energy Storage Materials. 24 (2020) 52–74. https://doi.org/10.1016/j.ensm.2019.07.031.

[11] H. Mehling, L.F. Cabeza, Heat and cold storage with PCM, Springer, Berlin, Heidelberg, 2008. https://doi.org/10.1007/978-3-540-68557-9.

[12] M. Neri, E. Chiavazzo, L. Mongibello, Numerical simulation and validation of commercial hot water tanks integrated with phase change material-based storage units, Journal of Energy Storage. 32 (2020) 101938. https://doi.org/10.1016/j.est.2020.101938.

[13] L. Hui, K. N'Tsoukpoe, L. Nolwenn, L. Lingai, Evaluation of a seasonal storage system of solar energy for house heating using different absorption couples, Energy Conversion and Management. 52 (2011) 2427–2436. https://doi.org/10.1016/j.enconman.2010.12.049.

[14] M. Rouhani, Sorption thermal energy storage for sustainable heating and cooling, School of Mechatronic Systems Engineering Faculty of Applied Science. (2019).

[15] A. de Gracia, L.F. Cabeza, Phase change materials and thermal energy storage for buildings, Energy and Buildings. 103 (2015) 414–419. https://doi.org/10.1016/j.enbuild.2015.06.007.

[16] A. Dahash, F. Ochs, M.B. Janetti, W. Streicher, Advances in seasonal thermal energy storage for solar district heating applications: A critical review on large-scale hot-water tank and pit thermal energy storage systems, Applied Energy. 239 (2019) 296–315. https://doi.org/10.1016/j.apenergy.2019.01.189.

[17] K. Faraj, M. Khaled, J. Faraj, F. Hachem, C. Castelain, Phase change material thermal energy storage systems for cooling applications in buildings: A review, Renewable and Sustainable Energy Reviews. 119 (2020) 109579. https://doi.org/10.1016/j.rser.2019.109579.

[18] N. Xie, Z. Huang, Z. Luo, X. Gao, Y. Fang, Z. Zhang, Inorganic salt hydrate for thermal energy storage, Applied Sciences (Switzerland). 7 (2017). https://doi.org/10.3390/app7121317.

[19] D.G. Atinafu, B.Y. Yun, S. Yang, H. Yuk, S. Wi, S. Kim, Structurally advanced hybrid support composite phase change materials: Architectural synergy, Energy Storage Materials. 42 (2021) 164–184. https://doi.org/10.1016/j.ensm.2021.07.022.

[20] M.Q. Wu, S. Wu, Y.F. Cai, R.Z. Wang, T.X. Li, Form-stable phase change composites: Preparation, performance, and applications for thermal energy conversion, storage and management, Energy Storage Materials. 42 (2021) 380–417. https://doi.org/10.1016/j.ensm.2021.07.019.

[21] K.E. N'Tsoukpoe, H. Liu, N. [Le Pierrès, L. Luo, A review on long-term sorption solar energy storage, Renewable and Sustainable Energy Reviews. 13 (2009) 2385–2396. https://doi.org/10.1016/j.rser.2009.05.008.

[22] G. Raj, Surface Chemistry, Krishna Prakashan Media (P) Ltd, n.d.

[23] N. Kharal, Selection of Novel Technology for Wastewater Tretment, Mathematical Sciences and Technology. (2017) 1–23. https://doi.org/10.13140/RG.2.2.32046.41286.

[24] L. Scapino, H.A. Zondag, J. Van Bael, J. Diriken, C.C.M. Rindt, Energy density and storage capacity cost comparison of conceptual solid and liquid sorption seasonal heat storage systems for low-temperature space heating, Renewable and Sustainable Energy Reviews. 76 (2017) 1314–1331. https://doi.org/10.1016/j.rser.2017.03.101.

[25] H.O. Helaly, M.M. Awad, I.I. El-Sharkawy, A.M. Hamed, Theoretical and experimental investigation of the performance of adsorption heat storage system, Applied Thermal Engineering. 147 (2019) 10–28. https://doi.org/10.1016/j.applthermaleng.2018.10.059.

[26] A. Frazzica, A. Freni, Adsorbent working pairs for solar thermal energy storage in buildings, Renewable Energy. 110 (2017) 87–94. https://doi.org/10.1016/j.renene.2016.09.047.

[27] V. Palomba, A. Frazzica, Comparative analysis of thermal energy storage technologies through the definition of suitable key performance indicators, Energy and Buildings. 185 (2019) 88–102. https://doi.org/10.1016/j.enbuild.2018.12.019.

[28] C. Del Pero, N. Aste, H. Paksoy, F. Haghighat, S. Grillo, F. Leonforte, Energy storage key performance indicators for building application, Sustainable Cities and Society. 40 (2018) 54–65. https://doi.org/10.1016/j.scs.2018.01.052.

[29] S. Wu, 4 - Heat energy storage and cooling in buildings, in: M.R. Hall (Ed.), Materials for Energy Efficiency and Thermal Comfort in Buildings, Woodhead Publishing, 2010: pp. 101–126. https://doi.org/10.1533/9781845699277.1.101.

[30] I. Sarbu, C. Sebarchievici, A Comprehensive Review of Thermal Energy Storage, Sustainability. 10 (2018) 191. https://doi.org/10.3390/su10010191.

[31] Y. Cui, J. Xie, J. Liu, S. Pan, Review of Phase Change Materials Integrated in Building Walls for Energy Saving, Procedia Engineering. 121 (2015) 763–770. https://doi.org/10.1016/j.proeng.2015.09.027.

[32] S.Z. Xu, R.Z. Wang, L.W. Wang, J. Zhu, Performance characterizations and thermodynamic analysis of magnesium sulfate-impregnated zeolite 13X and activated alumina composite sorbents for thermal energy storage, Energy. 167 (2019) 889–901. https://doi.org/10.1016/j.energy.2018.10.200.

[33] M. Fasano, M. Bozorg Bigdeli, M.R. Vaziri Sereshk, E. Chiavazzo, P. Asinari, Thermal transmittance of carbon nanotube networks: Guidelines for novel thermal storage systems and polymeric material of thermal interest, Renewable and Sustainable Energy Reviews. 41 (2015) 1028–1036. https://doi.org/10.1016/j.rser.2014.08.087.

[34] E. Chiavazzo, P. Asinari, Reconstruction and modeling of 3D percolation networks of carbon fillers in a polymer matrix, International Journal of Thermal Sciences. 49 (2010) 2272–2281. https://doi.org/10.1016/j.ijthermalsci.2010.07.019.

[35] M. Sangermano, L. Calvara, E. Chiavazzo, L. Ventola, P. Asinari, V. Mittal, R. Rizzoli, L. Ortolani, V. Morandi, Enhancement of electrical and thermal conductivity of Su-8 photocrosslinked coatings containing graphene, Progress in Organic Coatings. 86 (2015) 143–146. https://doi.org/10.1016/j.porgcoat.2015.04.023.

[36] M. Fasano, D. Borri, A. Cardellini, M. Alberghini, M. Morciano, E. Chiavazzo, P. Asinari, Multiscale simulation approach to heat and mass transfer properties of nanostructured materials for sorption heat storage, Energy Procedia. 126 (2017) 509–516. https://doi.org/10.1016/j.egypro.2017.08.229.

[37] A. [Fopah Lele, K.E. N'Tsoukpoe, T. Osterland, F. Kuznik, W.K.L. Ruck, Thermal conductivity measurement of thermochemical storage materials, Applied Thermal Engineering. 89 (2015) 916–926. https://doi.org/10.1016/j.applthermaleng.2015.06.077.

[38] H. Ibrahim, A. Ilinc, Techno-Economic Analysis of Different Energy Storage Technologies, in: A. Zobaa (Ed.), Energy Storage - Technologies and Applications, InTech, 2013. https://doi.org/10.5772/52220.

[39] S. Kalaiselvam, R. Parameshwaran, Chapter 4 - Sensible Thermal Energy Storage, in: S. Kalaiselvam, R. Parameshwaran (Eds.), Thermal Energy Storage Technologies for Sustainability, Academic Press, Boston, 2014: pp. 65–81. https://doi.org/10.1016/B978-0-12-417291-3.00004-9.

[40] N. Yu, R.Z. Wang, L.W. Wang, Sorption thermal storage for solar energy, Progress in Energy and Combustion Science. 39 (2013) 489–514. https://doi.org/10.1016/j.pecs.2013.05.004.

[41] V. Inglezakis, A. Zorpas, Heat of adsorption, adsorption energy and activation energy in adsorption and ion exchange systems, Desalination and Water Treatment - DESALIN WATER TREAT. 39 (2012) 149–157. https://doi.org/10.1080/19443994.2012.669169.

[42] M. Fasano, G. Falciani, V. Brancato, V. Palomba, P. Asinari, E. Chiavazzo, A. Frazzica, Atomistic modelling of water transport and adsorption mechanisms in silicoaluminophosphate for thermal energy storage, Applied Thermal Engineering. 160 (2019) 114075. https://doi.org/10.1016/j.applthermaleng.2019.114075.

[43] M. Fasano, D. Borri, E. Chiavazzo, P. Asinari, Protocols for atomistic modeling of water uptake into zeolite crystals for thermal storage and other applications, Applied Thermal Engineering. 101 (2016) 762–769. https://doi.org/10.1016/j.applthermaleng.2016.02.015.

[44] Q. Chang, Chapter 10 - Surface of Solids, in: Q. Chang (Ed.), Colloid and Interface Chemistry for Water Quality Control, Academic Press, 2016: pp. 175–225. https://doi.org/10.1016/B978-0-12-809315-3.00010-4.

[45] K. Oura, V.G. Lifshits, A.A. Saranin, A.V. Zotov, M. Katayama, Surface science: an introduction, Springer Science & Business Media, 2013.

[46] H. Liu, L. Long, X. Weng, S. Zheng, Z. Xu, Efficient removal of tetrabromobisphenol A using microporous and mesoporous carbons: The role of pore structure, Microporous and Mesoporous Materials. 298 (2020) 110052. https://doi.org/10.1016/j.micromeso.2020.110052.

[47] M.R. Usman, M. Saleem, R. Aslam, Chemical Engineering Terminology, Lulu.com, 2015. https://books.google.it/books?id=EgfECQAAQBAJ.

[48] S. Brunauer, P.H. Emmett, E. Teller, Adsorption of Gases in Multimolecular Layers, J. Am. Chem. Soc. 60 (1938) 309–319. https://doi.org/10.1021/ja01269a023.

[49] F. Ambroz, T.J. Macdonald, V. Martis, I.P. Parkin, Evaluation of the BET Theory for the Characterization of Meso and Microporous MOFs, Small Methods. 2 (2018) 1800173. https://doi.org/10.1002/smtd.201800173.

[50] Adsorption, in: Physics and Chemistry of Interfaces, John Wiley & Sons, Ltd, 2003: pp. 177–205. https://doi.org/10.1002/3527602313.ch9.

[51] S. Lowell, J.E. Shields, Adsorption isotherms, in: Powder Surface Area and Porosity, Springer, 1991: pp. 11–13.

[52] M. Thommes, K. Kaneko, A.V. Neimark, J.P. Olivier, F. Rodriguez-Reinoso, J. Rouquerol, K.S. Sing, Physisorption of gases, with special reference to the evaluation of surface area and pore size distribution (IUPAC Technical Report), Pure and Applied Chemistry. 87 (2015) 1051–1069.

[53] G. Trezza, L. Bergamasco, M. Fasano, E. Chiavazzo, Minimal crystallographic descriptors of sorption properties in hypothetical MOFs and role in sequential learning optimization, Npj Computational Materials. 8 (2022) 123. https://doi.org/10.1038/s41524-022-00806-7.

[54] K.C. Ng, H.T. Chua, C.Y. Chung, C.H. Loke, T. Kashiwagi, A. Akisawa, B.B. Saha, Experimental investigation of the silica gel-water adsorption isotherm characteristics, Applied Thermal Engineering. 21 (2001) 1631–1642. https://doi.org/10.1016/S1359-4311(01)00039-4.

[55] G.D. Chukin, V.I. Malevich, Structure of silica, Journal of Structural Chemistry. 18 (1977) 76–83. https://doi.org/10.1007/BF00745434.

[56] A. Feng, B.J. McCoy, Z.A. Munir, D.E. Cagliostro, Water Adsorption and Desorption Kinetics on Silica Insulation, Journal of Colloid and Interface Science. 180 (1996) 276–284. https://doi.org/10.1006/jcis.1996.0300.

[57] K.-S. Chang, H.-C. Wang, T.-W. Chung, Effect of regeneration conditions on the adsorption dehumidification process in packed silica gel beds, Applied Thermal Engineering - APPL THERM ENG. 24 (2004) 735–742. https://doi.org/10.1016/j.applthermaleng.2003.11.003.

[58] M. Matsuda, Application 25 - Zeolite Membrane, in: M. Naito, T. Yokoyama, K. Hosokawa, K. Nogi (Eds.), Nanoparticle Technology Handbook (Third Edition), Third Edition, Elsevier, 2018: pp. 539–542. https://doi.org/10.1016/B978-0-444-64110-6.00032-9.

[59] M. Fasano, T. Humplik, A. Bevilacqua, M. Tsapatsis, E. Chiavazzo, E.N. Wang, P. Asinari, Interplay between hydrophilicity and surface barriers on water transport in zeolite membranes, Nature Communications. 7 (2016) 12762. https://doi.org/10.1038/ncomms12762.

[60] C. Beauvais, A. Boutin, A.H. Fuchs, Adsorption of water in zeolite sodium-faujasite: A molecular simulation study, Comptes Rendus Chimie. 8 (2005) 485–490. https://doi.org/10.1016/j.crci.2004.11.011.

[61] S.K. Henninger, F.P. Schmidt, H.M. Henning, Characterisation and improvement of sorption materials with molecular modeling for the use in heat transformation applications, in: Adsorption, Springer, 2011: pp. 833–843. https://doi.org/10.1007/s10450-011-9342-6.

[62] W. Lutz, H. Toufar, D. Heidemann, N. Salman, C. Rüscher, T. Gesing, J.-C. Buhl, R. Bertram, Siliceous extra-framework species in dealuminated Y zeolites generated by steaming, Microporous and Mesoporous Materials. 104 (2007) 171–178. https://doi.org/10.1016/j.micromeso.2007.01.028.

[63] B.L. Meyers, T.H. Fleisch, C.L. Marshall, Dealumination and aluminum ion migration in faujasites, Applied Surface Science. 26 (1986) 503–516. https://doi.org/10.1016/0169-4332(86)90122-4.

[64] A. Jentys, G. Warecka, M. Derewinski, J. Lercher, Adsorption of water on ZSM 5 zeolites, The Journal of Physical Chemistry. 93 (1989). https://doi.org/10.1021/j100349a032.

[65] J. Jänchen, D. Ackermann, H. Stach, W. Brösicke, Studies of the water adsorption on Zeolites and modified mesoporous materials for seasonal storage of solar heat, Solar Energy. 76 (2004) 339–344. https://doi.org/10.1016/j.solener.2003.07.036.

[66] Hauer, Thermal enery storage with zeolite for heating and cooling application, Proceedings of the International Sorption Heat Pump Conference. (2002).

[67] H. Kerskes, B. Mette, S. Asenbeck, H. Drück, H. Müller-Steinhagen, Experimental and numerical investigations on thermo-chemical heat stoarge, in: Proceedings of the EUROSUN, 2010.

[68] H. Wu, P. Trens, B. Fraisse, F. Salles, J. Zajac, Hydration mechanism in Ce-exchanged zeolites and heat release performances upon adsorption of water vapour in support of their potential use in thermochemical storage of energy under mild conditions of adsorbent regeneration and saturation, Microporous and Mesoporous Materials. 296 (2020) 109999. https://doi.org/10.1016/j.micromeso.2020.109999.

[69] S.T. Wilson, B.M. Lok, C.A. Messina, T.R. Cannan, E.M. Flanigen, Aluminophosphate molecular sieves: a new class of microporous crystalline inorganic solids, Journal of the American Chemical Society. 104 (1982) 1146–1147. https://doi.org/10.1021/ja00368a062.

[70] X. Liu, N. Yan, L. Wang, C. Ma, P. Guo, P. Tian, G. Cao, Z. Liu, Landscape of AlPO-based structures and compositions in the database of zeolite structures, Microporous and Mesoporous Materials. 280 (2019). https://doi.org/10.1016/j.micromeso.2019.01.047.

[71] Database of Zeolite Structures, n.d. http://www.iza-structure.org/databases/ (accessed June 6, 2020).

[72] T. Kohler, M. Hinze, K. Müller, W. Schwieger, Temperature independent description of water adsorption on zeotypes showing a type V adsorption isotherm, Energy. 135 (2017) 227–236. https://doi.org/10.1016/j.energy.2017.06.115.

[73] C. Buttersack, Modeling of type IV and V sigmoidal adsorption isotherms, Phys. Chem. Chem. Phys. 21 (2019) 5614–5626. https://doi.org/10.1039/C8CP07751G.

[74] G. Poulet, P. Sautet, A. Tuel, Structure of Hydrated Microporous Aluminophosphates: Static and Molecular Dynamics Approaches of AlPO 4-34 from First Principles Calculations, (2002). https://doi.org/10.1021/jp020533p.

[75] A. Ristić, N.Z. Logar, S.K. Henninger, V. Kaučič, The Performance of Small-Pore Microporous Aluminophosphates in Low-Temperature Solar Energy Storage: The Structure-Property Relationship, Advanced Functional Materials. 22 (2012) 1952–1957. https://doi.org/10.1002/adfm.201102734.

[76] J. Bauer, T. Selvam, J. Ofili, E. Che, R. Herrmann, W. Schwieger, Stability of AlPO and SAPO molecular sieves during adsorption-desorption cycles of water vapor investigated by in-situ XRD measurements, in: R. Xu, Z. Gao, J. Chen, W. Yan (Eds.), From Zeolites to Porous MOF Materials - The 40th Anniversary of International Zeolite Conference, Elsevier, 2007: pp. 837–844. https://doi.org/10.1016/S0167-2991(07)80930-X.

[77] S.K. Henninger, G. Munz, K.-F. Ratzsch, P. Schossig, Cycle stability of sorption materials and composites for the use in heat pumps and cooling machines, Renewable Energy. 36 (2011) 3043–3049. https://doi.org/10.1016/j.renene.2011.03.032.

[78] M. Fischer, Water adsorption in SAPO-34: elucidating the role of local heterogeneities and defects using dispersion-corrected DFT calculations, Phys. Chem. Chem. Phys. 17 (2015) 25260–25271. https://doi.org/10.1039/C5CP04189A.

[79] C. Sun, Y. Wang, Z. Wang, H. Chen, X. Wang, H. Li, L. Sun, C. Fan, C. Wang, X. Zhang, Fabrication of hierarchical ZnSAPO-34 by alkali treatment with improved catalytic performance in the methanol-to-olefin reaction, Comptes Rendus Chimie. 21 (2018) 61–70. https://doi.org/10.1016/j.crci.2017.11.006.

[80] Minchev, Y. Neinska, V. Valtchev, V. Minkov, T. Tsoncheva, V. Penchev, H. Lechert, M. Hess, Effect of the rehydration on the acidity and catalytic activity of SAPO molecular sieves, Catalysis Letters. 18 (1993) 125–135. https://doi.org/10.1007/BF00769505.

[81] M. Briend, R. Vomscheid, M.J. Peltre, P.P. Man, D. Barthomeuf, Influence of the choice of the template on the short- and long-term stability of SAPO-34 zeolite, Journal of Physical Chemistry. 99 (1995) 8270–8276. https://doi.org/10.1021/j100020a060.

[82] M. Fischer, Interaction of water with (silico)aluminophosphate zeotypes: A comparative investigation using dispersion-corrected DFT, Physical Chemistry Chemical Physics. 18 (2016) 15738–15750. https://doi.org/10.1039/c6cp02289h.

[83] V. Brancato, A. Frazzica, Characterisation and comparative analysis of zeotype water adsorbents for heat transformation applications, Solar Energy Materials and Solar Cells. 180 (2018) 91–102. https://doi.org/10.1016/j.solmat.2018.02.035.

[84] S.K. Henninger, F.P. Schmidt, H.-M. Henning, Water adsorption characteristics of novel materials for heat transformation applications, Applied Thermal Engineering. 30 (2010) 1692–1702. https://doi.org/10.1016/j.applthermaleng.2010.03.028.

[85] M. Safaei, M.M. Foroughi, N. Ebrahimpoor, S. Jahani, A. Omidi, M. Khatami, A review on metal-organic frameworks: Synthesis and applications, TrAC Trends in Analytical Chemistry. 118 (2019) 401–425. https://doi.org/10.1016/j.trac.2019.06.007.

[86] S.L. James, Metal-organic frameworks, Chem. Soc. Rev. 32 (2003) 276–288. https://doi.org/10.1039/B200393G.

[87] D. Liu, D. Zou, H. Zhu, J. Zhang, Mesoporous Metal–Organic Frameworks: Synthetic Strategies and Emerging Applications, Small. 14 (2018) 1801454. https://doi.org/10.1002/smll.201801454.

[88] K. Wang, K.N. Hui, K. San Hui, S. Peng, Y. Xu, Recent progress in metal–organic framework/graphene-derived materials for energy storage and conversion: design, preparation, and application, Chem. Sci. 12 (2021) 5737–5766. https://doi.org/10.1039/D1SC00095K.

[89] P.Z. Moghadam, A. Li, X.-W. Liu, R. Bueno-Perez, S.-D. Wang, S.B. Wiggin, P.A. Wood, D. Fairen-Jimenez, Targeted classification of metal–organic frameworks in the Cambridge structural database (CSD), Chem. Sci. 11 (2020) 8373–8387. https://doi.org/10.1039/D0SC01297A.

[90]   S. Chaemchuen, X. Xiao, N. Klomkliang, M. Yusubov, F. Verpoort, Tunable Metal–Organic Frameworks for Heat Transformation Applications, Nanomaterials. 8 (2018) 661. https://doi.org/10.3390/nano8090661.

[91]   P. Kuesgens, M. Rose, I. Senkovska, H. Froede, A. Heerwig, S. Siegle, S. Kaskel, Characterization of Metal-Organic Frameworks by Water Adsorption, Microporous and Mesoporous Materials. 120 (2009) 325–330. https://doi.org/10.1016/j.micromeso.2008.11.020.

[92]   M.F. de Lange, K.J.F.M. Verouden, T.J.H. Vlugt, J. Gascon, F. Kapteijn, Adsorption-Driven Heat Pumps: The Potential of Metal–Organic Frameworks, Chem. Rev. 115 (2015) 12205–12250. https://doi.org/10.1021/acs.chemrev.5b00059.

[93]   N. Burtch, H. Jasuja, K. Walton, Water Stability and Adsorption in Metal−Organic Frameworks, Chemical Reviews. 114 (2014). https://doi.org/10.1021/cr5002589.

[94]   C. Wang, X. Liu, N. Keser Demir, J.P. Chen, K. Li, Applications of water stable metal–organic frameworks, Chem. Soc. Rev. 45 (2016) 5107–5134. https://doi.org/10.1039/C6CS00362A.

[95]   M. Ding, X. Cai, H.-L. Jiang, Improving MOF stability: approaches and applications, Chem. Sci. 10 (2019) 10209–10230. https://doi.org/10.1039/C9SC03916C.

[96]   J.D. Carruthers, D.A. Payne, K.S.W. Sing, L.J. Stryker, Specific and nonspecific interactions in the adsorption of argon, nitrogen, and water vapor on oxides, Journal of Colloid and Interface Science. 36 (1971) 205–216. https://doi.org/10.1016/0021-9797(71)90165-2.

[97]   Y. Hua, B. Ugur, F. [Handan Tezel, Adsorbent screening for thermal energy storage application, Solar Energy Materials and Solar Cells. 196 (2019) 119–123. https://doi.org/10.1016/j.solmat.2019.01.052.

[98]   B.F. Ngouana W., A.G. Kalinichev, Structural Arrangements of Isomorphic Substitutions in Smectites: Molecular Simulation of the Swelling Properties, Interlayer Structure, and Dynamics of Hydrated Cs–Montmorillonite Revisited with New Clay Models, The Journal of Physical Chemistry C. 118 (2014) 12758–12773. https://doi.org/10.1021/jp500538z.

[99]   X.W. Liu, M. Hu, Y.H. Hu, Chemical composition and surface charge properties of montmorillonite, Journal of Central South University of Technology (English Edition). 15 (2008) 193–197. https://doi.org/10.1007/s11771-008-0037-4.

[100] O.M. Sadek, W.K. Mekhamer, Ca-montmorillonite clay as thermal energy storage material, Thermochimica Acta. 363 (2000) 47–54. https://doi.org/10.1016/S0040-6031(00)00598-0.

[101] E.J.M. Hensen, B. Smit, Why Clays Swell, The Journal of Physical Chemistry B. 106 (2002) 12664–12667. https://doi.org/10.1021/jp0264883.

[102] F. Salles, J.-M. Douillard, O. Bildstein, C. Gaudin, B. Prelot, J. Zajac, H. [Van Damme, Driving force for the hydration of the swelling clays: Case of montmorillonites saturated with alkaline-earth cations, Journal of Colloid and Interface Science. 395 (2013) 269–276. https://doi.org/10.1016/j.jcis.2012.12.050.

[103] A. Jabbari-Hichri, S. Bennici, A. Auroux, CaCl2-containing composites as thermochemical heat storage materials, Solar Energy Materials and Solar Cells. 172 (2017) 177–185. https://doi.org/10.1016/j.solmat.2017.07.037.

[104] H. [van Olphen, Thermodynamics of interlayer adsorption of water in clays. I.—Sodium vermiculite, Journal of Colloid Science. 20 (1965) 822–837. https://doi.org/10.1016/0095-8522(65)90055-3.

[105] V. Palomba, S. Vasta, A. Freni, Experimental testing of AQSOA FAM Z02/water adsorption system for heat and cold storage, Applied Thermal Engineering. 124 (2017) 967–974. https://doi.org/10.1016/j.applthermaleng.2017.06.085.

[106] A. Permyakova, S. Wang, E. Courbon, F. Nouar, N. Heymans, P. D'Ans, N. Barrier, P. Billemont, G. De Weireld, N. Steunou, M. Frère, C. Serre, Design of salt–metal organic framework composites for seasonal heat storage applications, J. Mater. Chem. A. 5 (2017) 12889–12898. https://doi.org/10.1039/C7TA03069J.

[107] R. AL-Dadah, S. Mahmoud, E. Elsayed, P. Youssef, F. Al-Mousawi, Metal-organic framework materials for adsorption heat pumps, Energy. 190 (2020) 116356. https://doi.org/10.1016/j.energy.2019.116356.

[108] C. Bales, P. Gantenbein, D. Jaehnig, H. Kerskes, M. Van Essen, R. Weber, H. Zondag, 031-chemical and sorption storage–results from IEA-SHC task 32, in: Eurosun, 2008: pp. 1–8.

[109] N. Yu, R.Z. Wang, Z.S. Lu, L.W. Wang, Development and characterization of silica gel–LiCl composite sorbents for thermal energy storage, Chemical Engineering Science. 111 (2014) 73–84. https://doi.org/10.1016/j.ces.2014.02.012.

[110] Y. Zhang, R. Wang, T. Li, Y. Zhao, Thermochemical Characterizations of Novel Vermiculite-LiCl Composite Sorbents for Low-Temperature Heat Storage, Energies. 9 (2016) 854. https://doi.org/10.3390/en9100854.

[111] H. Stach, J. Mugele, J. Jänchen, E. Weiler, Influence of Cycle Temperatures on the Thermochemical Heat Storage Densities in the Systems Water/Microporous and Water/Mesoporous Adsorbents, Adsorption. 11 (2005) 393–404. https://doi.org/10.1007/s10450-005-5405-x.

[112] C.P. Bales, P.Dr. rer. nat. Gantenbein, A. Hauer, H.K. Henning, D. Jaenig, H. Kerskes, T. Nuñez, K. Visscher, Thermal Properties of Materials for Thermo-chemical Storage of Solar Heat : Report B2 of Subtask B, 2005.

[113] H. Kim, H.J. Cho, S. Narayanan, S. Yang, H. Furukawa, S. Schiffres, X. Li, Y.B. Zhang, J. Jiang, O.M. Yaghi, E.N. Wang, Characterization of Adsorption Enthalpy of Novel Water-Stable Zeolites and Metal-Organic Frameworks, Scientific Reports. 6 (2016) 1–8. https://doi.org/10.1038/srep19097.

[114] A. Elsayed, E. Elsayed, R. AL-Dadah, S. Mahmoud, A. Elshaer, W. Kaialy, Thermal energy storage using metal–organic framework materials, Applied Energy. 186 (2017) 509–519. https://doi.org/10.1016/j.apenergy.2016.03.113.

[115] L.G. Gordeeva, M.V. Solovyeva, Y.I. Aristov, NH2-MIL-125 as a promising material for adsorptive heat transformation and storage, Energy. 100 (2016) 18–24. https://doi.org/10.1016/j.energy.2016.01.034.

[116] A. Sapienza, A. Velte, I. Girnik, A. Frazzica, G. Füldner, L. Schnabel, Y. Aristov, "Water - Silica Siogel" working pair for adsorption chillers: Adsorption equilibrium and dynamics, Renewable Energy. 110 (2017) 40–46. https://doi.org/10.1016/j.renene.2016.09.065.

[117] A. Serbezov, J.D. Moore, Y. Wu, Adsorption Equilibrium of Water Vapor on Selexsorb-CDX Commercial Activated Alumina Adsorbent, J. Chem. Eng. Data. 56 (2011) 1762–1769. https://doi.org/10.1021/je100473f.

[118] X. Zheng, Z. Lin, B.Y. Xu, Thermal conductivity and sorption performance of nano-silver powder/FAPO-34 composite fin, Applied Thermal Engineering. 160 (2019) 114055. https://doi.org/10.1016/j.applthermaleng.2019.114055.

[119] Q. Gao, S. Han, Q. Ye, S. Cheng, T. Kang, H. Dai, Effects of Lanthanide Doping on the Catalytic Activity and Hydrothermal Stability of Cu-SAPO-18 for the Catalytic Removal of NOx (NH3-SCR) from Diesel Engines, Catalysts. 10 (2020) 336. https://doi.org/10.3390/catal10030336.

[120] C. Charalambous, G. Santori, E. Vilarrasa-Garcia, M. Bastos-Neto, C.L. Cavalcante, S. Brandani, Pure and Binary Adsorption of Carbon Dioxide and Nitrogen on AQSOA FAM Z02, J. Chem. Eng. Data. 63 (2018) 661–670. https://doi.org/10.1021/acs.jced.7b00864.

[121] M. Rouhani, W. Huttema, M. Bahrami, Thermal conductivity of AQSOA FAM-Z02 packed bed adsorbers in open and closed adsorption thermal energy storage systems, International Journal of Refrigeration. 105 (2019) 158–168. https://doi.org/10.1016/j.ijrefrig.2018.05.012.

[122] C.G. Bastos Andrade, S.M. Toffoli, F.R. Valenzuela Diaz, Adsorption and Surface Area of Modified Bentonite Used as Bleaching Clay, in: B. Li, J. Li, S. Ikhmayies, M. Zhang, Y.E. Kalay, J.S. Carpenter, J.-Y. Hwang, S.N. Monteiro, D. Firrao, A. Brown, C. Bai, Z. Peng,

J.P. Escobedo-Diaz, R. Goswami, J. Kim (Eds.), Characterization of Minerals, Metals, and Materials 2018, Springer International Publishing, Cham, 2018: pp. 333–341.

[123] E. Alvarez, N. Guillou, C. Martineau, B. Bueken, B. Van de Voorde, C. Le Guillouzer, P. Fabry, F. Nouar, F. Taulelle, D. de Vos, J.-S. Chang, K.H. Cho, N. Ramsahye, T. Devic, M. Daturi, G. Maurin, C. Serre, The Structure of the Aluminum Fumarate Metal–Organic Framework A520, Angewandte Chemie International Edition. 54 (2015) 3664–3668. https://doi.org/10.1002/anie.201410459.

[124] J. Temuujin, K. Okada, K.J.D. MacKenzie, Preparation of porous silica from vermiculite by selective leaching, Applied Clay Science. 22 (2003) 187–195. https://doi.org/10.1016/S0169-1317(02)00158-8.

[125] A.R. Sowunmi, C.O. Folayan, F.O. Anafi, O.A. Ajayi, N.O. Omisanya, D.O. Obada, D. Dodoo-Arhin, Dataset on the comparison of synthesized and commercial zeolites for potential solar adsorption refrigerating system, Data in Brief. 20 (2018) 90–95. https://doi.org/10.1016/j.dib.2018.07.040.

[126] A.J.H. McGaughey, M. Kaviany, Thermal conductivity decomposition and analysis using molecular dynamics simulations: Part II. Complex silica structures, International Journal of Heat and Mass Transfer. 47 (2004) 1799–1816. https://doi.org/10.1016/j.ijheatmasstransfer.2003.11.009.

[127] M. Ansari, A. Aroujalian, A. Raisi, B. Dabir, M. Fathizadeh, Preparation and characterization of nano-NaX zeolite by microwave assisted hydrothermal method, Advanced Powder Technology. 25 (2014) 722–727. https://doi.org/10.1016/j.apt.2013.10.021.

[128] M.B. Jakubinek, B.-Z. Zhan, M.A. White, Temperature-dependent thermal conductivity of powdered zeolite NaX, Microporous and Mesoporous Materials. 103 (2007) 108–112. https://doi.org/10.1016/j.micromeso.2007.01.040.

[129] L. Wang, M. Gandorfer, T. Selvam, W. Schwieger, Determination of faujasite-type zeolite thermal conductivity from measurements on porous composites by laser flash method, Materials Letters. 221 (2018) 322–325. https://doi.org/10.1016/j.matlet.2018.03.157.

[130] S.N. Khalifah, Z.N. aini, E.K. Hayati, N. Aini, A. Prasetyo, Synthesis and characterization of mesoporous NaY zeolite from natural Blitar's kaolin, IOP Conf. Ser.: Mater. Sci. Eng. 333 (2018) 012005. https://doi.org/10.1088/1757-899X/333/1/012005.

[131] F. Koçyigit, E. Kavak Akpinar, Y. Biçer, Experimental and theoretical study for the determination of thermal conductivity of porous building material made with pumice and tragacanth, Journal of Adhesion Science and Technology. 30 (2016) 2357–2371. https://doi.org/10.1080/01694243.2016.1182832.

[132] H. Furukawa, F. Gándara, Y.-B. Zhang, J. Jiang, W.L. Queen, M.R. Hudson, O.M. Yaghi, Water Adsorption in Porous Metal–Organic Frameworks and Related Materials, J. Am. Chem. Soc. 136 (2014) 4369–4381. https://doi.org/10.1021/ja500330a.

[133] A. Terzis, A. Ramachandran, K. Wang, M. Asheghi, K.E. Goodson, J.G. Santiago, High-Frequency Water Vapor Sorption Cycling Using Fluidization of Metal-Organic Frameworks, Cell Reports Physical Science. 1 (2020) 100057. https://doi.org/10.1016/j.xcrp.2020.100057.

[134] P.A.J. Donkers, L.C. Sögütoglu, H.P. Huinink, H.R. Fischer, O.C.G. Adan, A review of salt hydrates for seasonal heat storage in domestic applications, Applied Energy. 199 (2017) 45–68. https://doi.org/10.1016/j.apenergy.2017.04.080.

[135] A. Fopah-Lele, J.G. Tamba, A review on the use of $SrBr_2 \cdot 6H_2O$ as a potential material for low temperature energy storage systems and building applications, Solar Energy Materials and Solar Cells. 164 (2017) 175–187. https://doi.org/10.1016/j.solmat.2017.02.018.

[136] A.R. Kamali, D.J. Fray, C. Schwandt, Thermokinetic characteristics of lithium chloride, Journal of Thermal Analysis and Calorimetry. 104 (2011) 619–626. https://doi.org/10.1007/s10973-010-1045-9.

[137] T. Li, R. Wang, J.K. Kiplagat, A target-oriented solid-gas thermochemical sorption heat transformer for integrated energy storage and energy upgrade, AIChE Journal. 59 (2013) 1334–1347. https://doi.org/10.1002/aic.13899.

[138] B. Spinner, Ammonia-based thermochemical transformers, Heat Recovery Systems and CHP. 13 (1993) 301–307. https://doi.org/10.1016/0890-4332(93)90053-X.

[139] K.S. Babu, E.A. Kumar, Thermodynamic analysis of compressor operated resorption thermochemical energy storage system for heat storage, combined cooling and heat upgradation, Journal of Energy Storage. 50 (2022) 104659. https://doi.org/10.1016/j.est.2022.104659.

[140] A. Mehari, Z.Y. Xu, R.Z. Wang, Thermal energy storage using absorption cycle and system: A comprehensive review, Energy Conversion and Management. 206 (2020) 112482. https://doi.org/10.1016/j.enconman.2020.112482.

[141] R. Sharma, E. Anil Kumar, Study of ammoniated salts based thermochemical energy storage system with heat up-gradation: A thermodynamic approach, Energy. 141 (2017) 1705–1716. https://doi.org/10.1016/j.energy.2017.11.015.

[142] T. Yan, R.Z. Wang, T.X. Li, L.W. Wang, I.T. Fred, A review of promising candidate reactions for chemical heat storage, Renewable and Sustainable Energy Reviews. 43 (2015) 13–31. https://doi.org/10.1016/j.rser.2014.11.015.

[143] Y. Zhong, R.E. Critoph, R.N. Thorpe, Z. Tamainot-Telto, Yu.I. Aristov, Isothermal sorption characteristics of the BaCl2–NH3 pair in a vermiculite host matrix, Applied Thermal Engineering. 27 (2007) 2455–2462. https://doi.org/10.1016/j.applthermaleng.2007.02.011.

[144] J.V. Veselovskaya, R.E. Critoph, R.N. Thorpe, S. Metcalf, M.M. Tokarev, Yu.I. Aristov, Novel ammonia sorbents "porous matrix modified by active salt" for adsorptive heat transformation: 3. Testing of "BaCl2/vermiculite" composite in a lab-scale adsorption chiller, Applied Thermal Engineering. 30 (2010) 1188–1192. https://doi.org/10.1016/j.applthermaleng.2010.01.035.

[145] Y.J. Zhao, R.Z. Wang, Y.N. Zhang, N. Yu, Development of SrBr2 composite sorbents for a sorption thermal energy storage system to store low-temperature heat, Energy. 115 (2016) 129–139. https://doi.org/10.1016/j.energy.2016.09.013.

[146] Y. Yuan, H. Bao, Z. Ma, Y. Lu, A.P. Roskilly, Investigation of equilibrium and dynamic performance of SrCl2-expanded graphite composite in chemisorption refrigeration system, Applied Thermal Engineering. 147 (2019) 52–60. https://doi.org/10.1016/j.applthermaleng.2018.10.071.

[147] H. Bao, Z. Ma, Thermochemical energy storage, in: Storing Energy, Elsevier, 2022: pp. 651–683. https://doi.org/10.1016/B978-0-12-824510-1.00028-3.

[148] S. Hinmers, G.H. Atkinson, R.E. Critoph, M. van der Pal, Modelling and Analysis of Ammonia Sorption Reactions in Halide Salts, International Journal of Refrigeration. 137 (2022) 188–211. https://doi.org/10.1016/j.ijrefrig.2022.01.032.

[149] R. Iwata, T. Yamauchi, Y. Hirota, M. Aoki, T. Shimazu, Reaction kinetics of ammonia absorption/desorption of metal salts, Applied Thermal Engineering. 72 (2014) 244–249. https://doi.org/10.1016/j.applthermaleng.2014.07.034.

[150] H. Bao, Z. Ma, A.P. Roskilly, Kinetic Models of Salt-Ammonia Chemisorption: An Overview and Comparison, Chemisorption: Properties, Reactions and Uses. (2018).

[151] Y.I. Aristov, G. Restuccia, G. Cacciola, V.N. Parmon, A family of new working materials for solid sorption air conditioning systems, Applied Thermal Engineering. 22 (2002) 191–204. https://doi.org/10.1016/S1359-4311(01)00072-2.

[152] L. Gordeeva, A. Freni, T. Krieger, G. Restuccia, Y. Aristov, Composites "lithium halides in silica gel pores": Methanol sorption equilibrium, Microporous and Mesoporous Materials. 112 (2008) 254–261. https://doi.org/10.1016/j.micromeso.2007.09.040.

[153] I. Simonova, A. Freni, G. Restuccia, Y. Aristov, Water sorption on composite "silica modified by calcium nitrate," Microporous and Mesoporous Materials - MICROPOROUS

MESOPOROUS MAT. 122 (2009) 223–228.
https://doi.org/10.1016/j.micromeso.2009.02.034.

[154] L.G. Gordeeva, Yu.I. Aristov, Composites 'salt inside porous matrix' for adsorption heat transformation: a current state-of-the-art and new trends, International Journal of Low-Carbon Technologies. 7 (2012) 288–302. https://doi.org/10.1093/IJLCT/CTS050.

[155] J.X. Xu, T.X. Li, J.W. Chao, T.S. Yan, R.Z. Wang, High energy-density multi-form thermochemical energy storage based on multi-step sorption processes, Energy. 185 (2019) 1131–1142. https://doi.org/10.1016/j.energy.2019.07.076.

[156] A.D. Grekova, L.G. Gordeeva, Y.I. Aristov, Composite "LiCl/vermiculite" as advanced water sorbent for thermal energy storage, Applied Thermal Engineering. 124 (2017) 1401–1408. https://doi.org/10.1016/j.applthermaleng.2017.06.122.

[157] E. Elsayed, R. AL-Dadah, S. Mahmoud, P. Anderson, A. Elsayed, Adsorption cooling system employing novel MIL-101(Cr)/CaCl2 composites: Numerical study, International Journal of Refrigeration. 107 (2019) 246–261. https://doi.org/10.1016/j.ijrefrig.2019.08.004.

[158] Y.N. Zhang, R.Z. Wang, Y.J. Zhao, T.X. Li, S.B. Riffat, N.M. Wajid, Development and thermochemical characterizations of vermiculite/SrBr2 composite sorbents for low-temperature heat storage, Energy. 115 (2016) 120–128. https://doi.org/10.1016/j.energy.2016.08.108.

[159] V. Brancato, L. Gordeeva, A. Sapienza, V. Palomba, S. Vasta, A. Grekova, A. Frazzica, Y. Aristov, Experimental characterization of the LiCl/Vermiculite composite for sorption heat storage applications, International Journal of Refrigeration. (2018). https://doi.org/10.1016/j.ijrefrig.2018.08.006.

[160] E. Marceau, X. Carrier, M. Che, Impregnation and Drying, in: Synthesis of Solid Catalysts, John Wiley & Sons, Ltd, 2009: pp. 59–82. https://doi.org/10.1002/9783527626854.ch4.

[161] L. Calabrese, V. Brancato, V. Palomba, A. Frazzica, L.F. Cabeza, Innovative composite sorbent for thermal energy storage based on a SrBr2·6H2O filled silicone composite foam, Journal of Energy Storage. 26 (2019) 100954. https://doi.org/10.1016/j.est.2019.100954.

[162] L. Lavagna, D. Burlon, R. Nisticò, V. Brancato, A. Frazzica, M. Pavese, E. Chiavazzo, Cementitious composite materials for thermal energy storage applications: a preliminary characterization and theoretical analysis, Sci Rep. 10 (2020) 12833. https://doi.org/10.1038/s41598-020-69502-0.

[163] A. Fopah Lele, K. Korhammer, N. Wegscheider, H.U. Rammelberg, T. Osterland, W. Ruck, Thermal conductivity measurement of salt hydrate as porous material using calorimetric (DSC) method, in: 2013. https://doi.org/10.13140/RG.2.1.3034.9927.

[164] L. Shere, S. Trivedi, S. Roberts, A. Sciacovelli, Y. Ding, Synthesis and Characterization of Thermochemical Storage Material Combining Porous Zeolite and Inorganic Salts, Heat Transfer Engineering. 40 (2019) 1176–1181. https://doi.org/10.1080/01457632.2018.1457266.

[165] S. Salviati, F. Carosio, G. Saracco, A. Fina, Hydrated Salt/Graphite/Polyelectrolyte Organic-Inorganic Hybrids for Efficient Thermochemical Storage, Nanomaterials. 9 (2019) 420. https://doi.org/10.3390/nano9030420.

[166] M. Gaeini, A.L. Rouws, J.W.O. Salari, H.A. Zondag, C.C.M. Rindt, Characterization of microencapsulated and impregnated porous host materials based on calcium chloride for thermochemical energy storage, Applied Energy. 212 (2018) 1165–1177. https://doi.org/10.1016/j.apenergy.2017.12.131.

[167] K. Korhammer, M.-M. Druske, A. Fopah-Lele, H.U. Rammelberg, N. Wegscheider, O. Opel, T. Osterland, W. Ruck, Sorption and thermal characterization of composite materials based on chlorides for thermal energy storage, Applied Energy. 162 (2016) 1462–1472. https://doi.org/10.1016/j.apenergy.2015.08.037.

[168] A. Cammarata, V. Verda, A. Sciacovelli, Y. Ding, Hybrid strontium bromide-natural graphite composites for low to medium temperature thermochemical energy storage: Formulation,

fabrication and performance investigation, Energy Conversion and Management. 166 (2018) 233–240. https://doi.org/10.1016/j.enconman.2018.04.031.

[169] A. Mehrabadi, M. Farid, New salt hydrate composite for low-grade thermal energy storage, Energy. 164 (2018) 194–203. https://doi.org/10.1016/j.energy.2018.08.192.

[170] A. Grekova, L. Gordeeva, Y. Aristov, Composite sorbents "Li/Ca halogenides inside Multi-wall Carbon Nano-tubes" for Thermal Energy Storage, Solar Energy Materials and Solar Cells. 155 (2016) 176–183. https://doi.org/10.1016/j.solmat.2016.06.006.

[171] A. Ristić, N.Z. Logar, New composite water sorbents CaCl2-PHTS for low-temperature sorption heat storage: Determination of structural properties, Nanomaterials. 9 (2019). https://doi.org/10.3390/nano9010027.

[172] E. Courbon, P. D'Ans, A. Permyakova, O. Skrylnyk, N. Steunou, M. Degrez, M. Frère, A new composite sorbent based on SrBr2 and silica gel for solar energy storage application with high energy storage density and stability, Applied Energy. 190 (2017) 1184–1194. https://doi.org/10.1016/j.apenergy.2017.01.041.

[173] E. Courbon, P. D'Ans, A. Permyakova, O. Skrylnyk, N. Steunou, M. Degrez, M. Frère, Further improvement of the synthesis of silica gel and CaCl2 composites: Enhancement of energy storage density and stability over cycles for solar heat storage coupled with space heating applications, Solar Energy. 157 (2017) 532–541. https://doi.org/10.1016/j.solener.2017.08.034.

[174] E. Piperopoulos, L. Calabrese, P. Bruzzaniti, V. Brancato, V. Palomba, A. Caprì, A. Frazzica, L.F. Cabeza, E. Proverbio, C. Milone, Morphological and Structural Evaluation of Hydration/Dehydration Stages of MgSO4 Filled Composite Silicone Foam for Thermal Energy Storage Applications, Applied Sciences. 10 (2020) 453. https://doi.org/10.3390/app10020453.

[175] S.P. Casey, D. Aydin, S. Riffat, J. Elvins, Salt impregnated desiccant matrices for 'open' thermochemical energy storage—Hygrothermal cyclic behaviour and energetic analysis by physical experimentation, Energy and Buildings. 92 (2015) 128–139. https://doi.org/10.1016/j.enbuild.2015.01.048.

[176] A. Sapienza, I.S. Glaznev, S. Santamaria, A. Freni, Y.I. Aristov, Adsorption chilling driven by low temperature heat: New adsorbent and cycle optimization, Applied Thermal Engineering. 32 (2012) 141–146. https://doi.org/10.1016/j.applthermaleng.2011.09.014.

[177] Y.I. Aristov, Current progress in adsorption technologies for low-energy buildings, Future Cities and Environment. 1 (2015) 10. https://doi.org/10.1186/s40984-015-0011-x.

[178] S. Hongois, F. Kuznik, P. Stevens, J.-J. Roux, Development and characterisation of a new MgSO4−zeolite composite for long-term thermal energy storage, Solar Energy Materials and Solar Cells. 95 (2011) 1831–1837. https://doi.org/10.1016/j.solmat.2011.01.050.

[179] T.S. Yan, T.X. Li, J.X. Xu, R.Z. Wang, Water sorption properties, diffusion and kinetics of zeolite NaX modified by ion-exchange and salt impregnation, International Journal of Heat and Mass Transfer. 139 (2019) 990–999. https://doi.org/10.1016/j.ijheatmasstransfer.2019.05.080.

[180] V. Palomba, A. Frazzica, Recent advancements in sorption technology for solar thermal energy storage applications, Solar Energy. 192 (2019) 69–105. https://doi.org/10.1016/j.solener.2018.06.102.

[181] M. Ashby, Preface, in: M.F. Ashby (Ed.), Materials Selection in Mechanical Design (Fourth Edition), Butterworth-Heinemann, Oxford, 2011: pp. xi–xii. https://doi.org/10.1016/B978-1-85617-663-7.00024-2.

[182] M. Alberghini, M. Morciano, M. Fasano, F. Bertiglia, V. Fernicola, P. Asinari, E. Chiavazzo, Multistage and passive cooling process driven by salinity difference, Sci. Adv. 6 (2020) eaax5015. https://doi.org/10.1126/sciadv.aax5015.